Muscle calcium stress cleaves junctophilin1, unleashing a gene regulatory program predicted to correct glucose dysregulation

Revision 1

Eshwar R. Tammineni[1], Lourdes Figueroa[1], Carlo Manno[1], Disha Varma[2], Natalia Kraeva[3], Carlos A Ibarra[3], Amira Klip[4], Sheila Riazi[3] and Eduardo Ríos[1]

[1]Department of Physiology and Biophysics, Rush University, Chicago, United States; [2]Department of Internal Medicine, Division of Nephrology, Rush University; [3]Department of Anesthesia & Pain Management, University of Toronto; 4 Cell Biology Program, The Hospital for Sick Children, Toronto, Canada.

Address for correspondence:

Eshwar R Tammineni

Rush University School of Medicine

1750 West Harrison Street, Suite 1279 JS

Chicago, IL 60612, USA

tammineni.er@gmail.com

Ph. 312 9428044 (office), 312 9426454 (Department)

312 4988423 (cell). Fax 312 9428711

Abstract

Calcium ion movements between cellular stores and the cytosol govern muscle contraction, the most energy-consuming function in mammals, which confers skeletal myofibers a pivotal role in glycemia regulation. Chronic myoplasmic calcium elevation, found in malignant hyperthermia-susceptible (MHS) patients and multiple myopathies, has been suggested to underlie the progression from hyperglycemia to insulin resistance. What drives such progression remains elusive. We find that muscle cells derived from MHS patients have increased an activated fragment of GSK3β — a specialized kinase that inhibits glycogen synthase, impairing glucose utilization and delineating a path to hyperglycemia. We also find decreased content of junctophilin1, an essential structural protein that colocalizes in the couplon with the voltage-sensing $Ca_V1.1$, the calcium channel RyR1 and calpain1, accompanied by an increase in a 44-kDa junctophilin1 fragment (JPh44) that moves into nuclei. We trace these changes to activated proteolysis by calpain1, secondary to increased myoplasmic calcium. We demonstrate that a JPh44-like construct induces transcriptional changes predictive of increased glucose utilization in myoblasts, including less transcription and translation of GSK3β and decreased transcription of proteins that reduce utilization of glucose. These effects reveal a stress-adaptive response, mediated by the novel regulator of transcription JPh44.

Introduction

In the excitation-contraction (EC) coupling process of striated muscles, action potential depolarization of the plasma or transverse (T) tubule membranes command the transient release of Ca^{2+} into the myoplasm, enabling muscle contraction. The crucial device in this process is the couplon, a physical continuum of proteins that includes dihydropyridine receptor (DHPR, $Ca_V1.1$), ryanodine receptor 1 (RyR1), FKBP12, junctophilin1 (JPh1), Stac3, junctin, triadin and calsequestrin, among other components (1,2).

Only 5 proteins are necessary to assemble a functional, skeletal muscle-type EC coupling system in expression models (3,4). One of them is junctophilin, JPh (5), with skeletal and cardiac isoforms (1 and 2) deemed essential for creating and maintaining the junctional structure (T-SR junctions, dyads or triads) characteristic of striated muscle (6,7).

Susceptibility to Malignant Hyperthermia (MHS (8)) is a condition paradigmatic of gain-of-function couplonopathies (9,10). The primary defect in MHS is an alteration of RyR1 or another couplon protein, which leads to an increase in resting or activated openness of the channel. The increased "leak" causes a reduction in free Ca^{2+} concentration and total Ca^{2+} content inside the SR, in turn leading to an increase in resting free Ca^{2+} concentration, $[Ca^{2+}]_{cyto}$ (11,12), secondary to changes in the plasma membrane in response to SR depletion (13–16). Duchenne Muscular Dystrophy (DMD) is another example of a condition that raises resting $[Ca^{2+}]_{cyto}$, albeit by different mechanisms (17–19)

MHS patients show other abnormalities, probably derived in many cases from the chronically elevated $[Ca^{2+}]_{cyto}$. They have altered musculoskeletal function (with pain, cramps, stiffness, muscle fatigue and bone deformity as common manifestations (20,21)), as well as systemic dysfunction. Notably, and possibly as a consequence of reduced uptake and processing of glucose by muscle (22), the frequency of hyperglycemia (23) and diabetes (22) is more than 2-fold greater in MHs patients than in the general age-matched population.

In 2013, Graham Lamb and coworkers reported the cleavage of JPh1 and 2 in skeletal muscle and JPh2 in cardiac muscle in the presence of high $[Ca^{2+}]_{cyto}$, and associated it to the activation of calpain 1 (24). In cardiac muscle, the junctophilin isoform JPh2 is known to have a function similar to that of JPh1 in skeletal muscle — maintain structural integrity of the T-SR junction or dyad (25–27). Strikingly, fragments of JPh2 have been shown to additionally work in regulation of gene expression within nuclei (28,29).

We now find that the content of full-size JPh1 is reduced in skeletal muscle of MHS patients, while a C-terminal, 44-kDa JPh1 fragment, which we refer to as JPh44, moves away from the triadic location of the full-size protein and relocates to the nucleus. The observations indicate that the increased cleavage of JPh1 in MHS patients is due to activation of calpain1 by their higher $[Ca^{2+}]_{cyto}$.

The proteolysis of JPh1, with possible de-stabilization of T-SR junctions (6,30), and the entry of its fragments into nuclei could contribute to the disease phenotype, as proposed for fragments of JPh2 produced in cardiac muscle of failing hearts (28,29). On the other hand, LS Song and colleagues (28,31) provided evidence that the intra-nuclear actions of JPh2 fragments are "stress-adaptive", partially offsetting the negative consequences of activation of proteolysis.

Given these precedents and the presence in the sequence of JPh44 of segments capable of interaction with DNA, here we tested the hypothesis that JPh44 exerts transcriptional control compensatory for the deleterious effects of elevated $[Ca^{2+}]_{cyto}$. The study demonstrates beneficial effects of the fragment on the transcription and translation of enzymes active in glucose utilization by skeletal muscle.

1 ## Results

2

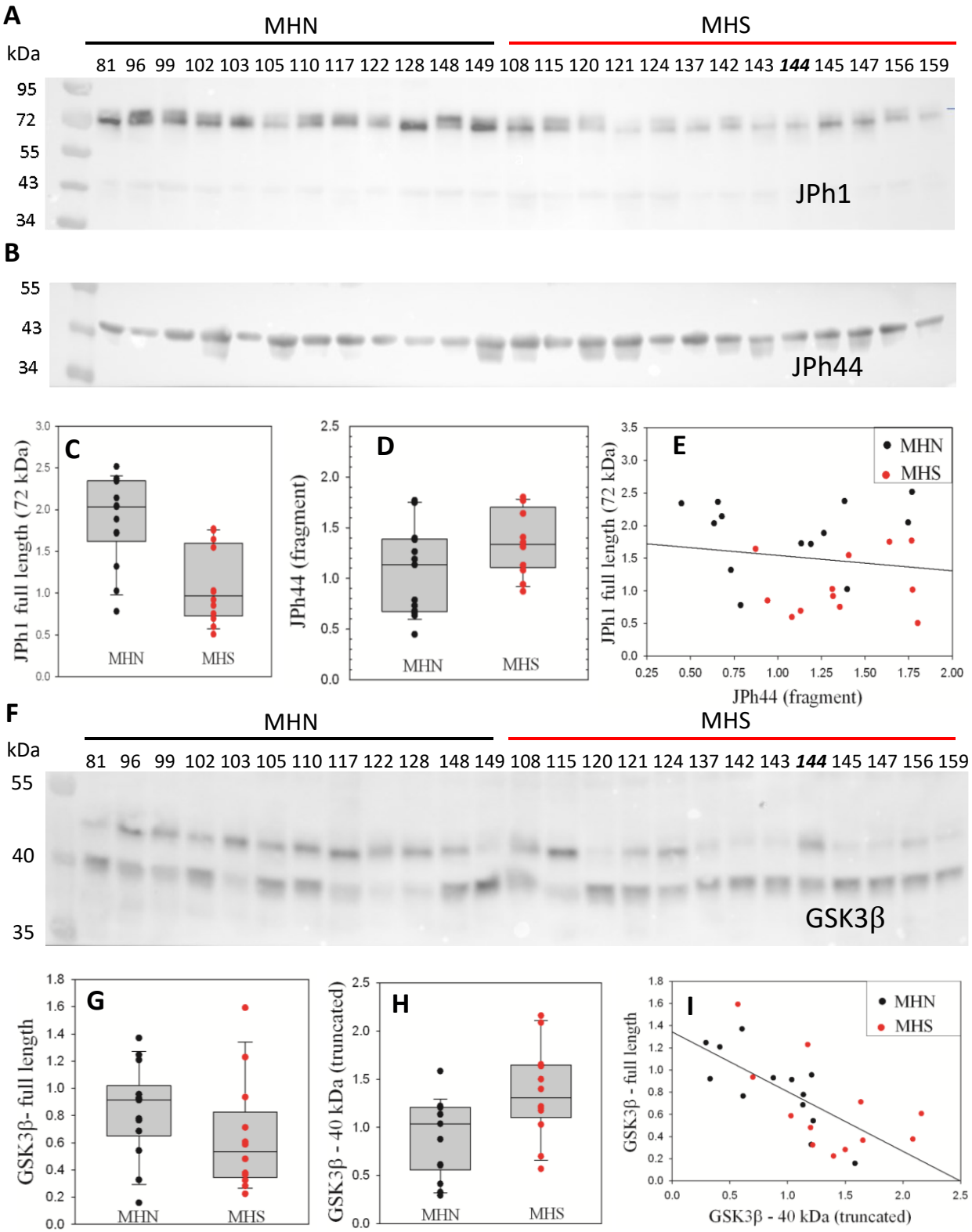

Figure 1. Fragmentation of proteins in MHS human muscle. A, Western blot (WB) of whole protein fraction from individual subjects' biopsies, stained with antibody A. Subjects were diagnosed as MHN or MHS as indicated. Numbers identify individuals. (Sample #144, an MHN, is misplaced). B, WB of a 2nd gel, using antibody B, which specifically stains JPh44 (see Supplemental fig.2 to Fig. 1). C, D, plots of signal in the 13 MHN and 12 MHS bands of panels A and B, respectively. p of no difference is < 0.001 and 0.06, respectively for JPh1 and JPh44. E, JPh1 vs JPh44 WB signals for all patients. The correlation is poor (R = -0.16). F, WB of whole protein fraction from the same biopsies, stained for GSK3β. G, H, box plots of the signal in the ~47 and ~40 kDa bands for MHN and MHS subjects. The difference is highly significant for the light band signal (p = 0.015) but not for the 47 kDa band (p = 0.14). I, 40 kDa vs. 47 kDa signals for all patients. The correlation is highly significant (R = -0.69, p < 0.001). *Data trace*. Raw data and statistical calculations in *GSK3β graphs and statistics.JNB*, sections 1 and 2. (all data in Harvard Dataverse described in Methods). See also 3 supplemental figures.

JPh1 is cleaved in MH-susceptible patients

A large increase in $[Ca^{2+}]_{cyto}$ has been found in muscle fibers from MHS individuals (12), myotubes derived from MHS patient biopsies (21) and in MHS animal models (11). MHS animals also showed increased calpain activity (32). Given that junctophilins are targets of Ca^{2+}-activated calpain proteases (28,29), we hypothesized that excess $[Ca^{2+}]_{cyto}$, by promotion of calpain activity, enhances JPh1 cleavage in MHS individuals. As a test, JPh1 was quantified by Western blotting (WB) on the same 25-lane gel, in total protein extracts from biopsied muscle of 13 MHN (normal) and 12 MHS subjects. The immunoblot, stained using a polyclonal antibody raised against a human JPh1 immunogen (residues 387-512), referred to here as "A", is shown in Fig. 1A. A visible reduction in the MHS of a ~72 kDa stained band revealed an almost 2-fold, statistically significant difference in content (Fig. 1C). Because the 72-75 kDa migration weight is consistent with the full JPh1 sequence, we refer to this band as "JPh1". That the band is in some columns a doublet, and that it migrates slightly faster than the corresponding band in mouse muscle gels (Supplement Fig. 1 to Fig. 1) indicates that proteolytic degradation may take place in the human biopsies and this band may not correspond to the full sequence of JPh1.

A blot from a different gel, stained with anti-JPh1 antibody "B" (raised against a more distal mouse JPh1 immunogen, 509-622) showed a greater content of a band with an effective migration size of ~44 kDa, referred to as JPh44 (Fig. 1B, D, $p = 0.06$). Blots in Supplemental Fig. 2 to Fig. 1 demonstrate that ab A reacts with both JPh1 and JPh44, while ab B fails to react with the 72 kDa protein, therefore constituting a useful tool for detection of JPh44 by immunofluorescence. The 72 kDa protein is overwhelmingly more abundant than its fragments, including JPh44 in nearly every condition (as shown in Fig. 1, its supplemental Fig. 2 and multiple documents later). Accordingly, the fluorescence of ab A can be used as a monitor of JPh1, with minimal error. Herein and unless noted differently, the labels "JPh1" and "JPh44" tag images of fluorescence of ab A and B, respectively.

While these results suggest that a greater cleavage of JPh1 leads to a reduction in its content, with consequent increase in the 44 kDa fragment, there is a poor negative correlation in individual subjects between the two changes (Fig. 1E). A tentative explanation is that the cleavage process, which may operate at multiple sites and sequentially on cleaved products, results in faster degradation of the full protein, blurring any detailed correspondence between its disappearance and the increase in content of some fragments.

Fragmentation of glycogen synthase kinase 3 (GSK3β) is increased in MHS patients

Phosphorylase kinase (PhK) reciprocally activates glycogen phosphorylase and inhibits glycogen synthase (GS). In previous work we demonstrated that this enzyme is activated in the muscle of MHS patients(22). Its effects are consistent with an observed shift of the glycogen ←→ glucose balance towards glycogenolysis (22), which is presumed responsible for the hyperglycemia and diabetes that develops in many of these patients (22,23). Here we compared the contents of GSK3β, a serine/threonine protein kinase that directly inhibits GS by phosphorylation. The kinase activity of GSK3β is controlled by its phosphorylation at Ser 9 and also promoted by truncation of the original ~47 kDa molecule to a form of ~40 kDa (33–35).

WB of protein extracts (Fig. 1F) from muscle biopsies of the same patients of Fig. 1A, reveal both forms of GSK3β. The signal in the 47-kDa band of full-size GSK3β was reduced in MHS, while that of the activated 40-kDa fragment was increased. The changes in the two proteins were highly negatively correlated (Fig. 1I); consequently, the ratio of signals (40-kDa/47-kDa) was more than 3-fold greater in the MHS group, with high statistical significance. Regardless of

diagnosis (MHS or MHN), there was a significant positive correlation between content of the activated GSK3β form and serum glucose (supplemental Fig. 3 to Fig. 1). These results are consistent with activation of the GS kinase by calpain proteolysis, which contributes to the shift in glycogen ←→ glucose balance in favor of glycogenolysis, presumably by inhibitory phosphorylation of GS.

Localization of the 44 kDa fragment of JPh1in skeletal muscle

In cardiac muscle, the full-length JPh2 protein is located at terminal cisternae of the SR, while cleaved JPh2 fragments can be found inside nuclei (28,29). Here we defined the location of JPh1 and JPh44 by immunostaining combined with 3D high-resolution imaging (a procedure used for every fluorescence image shown in this study, consisting in acquisition of vertical "*z*-stacks" of confocal *x-y* images, followed by a correction algorithm described in Methods). Moderately stretched thin myofiber bundles were fixed in PFA and stained with antibodies A or B. As shown in Fig. 2 (panels A), the ab A signal was largely located at T-SR junctions, where it was highly colocalized with RyR1. In contrast, ab B (JPh44-specific) detected discrete particles at variable locations within the sarcomeric I band, as well as nuclei (panel 2Bb), and accordingly failed to colocalize with Ry1 (panels 2Cc, Cd).

Colocalization between the junctophilin forms and RyR1 was quantified by four measures, with average results listed in Table 1. First: R, Pearson's correlation coefficient of immunofluorescence intensities, calculated pixel by pixel after subtraction of a small background signal. This index had high value for the ab A fluorescence, (indicating a much greater quantity of full-size JPh1 than JPh44) and low for ab B (JPh44), with high statistical significance of the difference. Second: the Intensity Correlation Quotient (ICQ), emergent from an approach by Li et al. (36) illustrated in panel 2Cb, whereby the intensity of fluorescence of ab A (JPh1) is plotted, pixel by pixel, against the covariance of ab A and RyR1 intensities (Methods). The comma-shaped cloud with negative curvature, shown in 2Cb, is a characteristic of high colocalization, contrasting with the funnel-shaped cloud found for ab B vs RyR1 (panel 2Cd), which includes pixels with negative covariance, reflecting mutual exclusion rather than colocalization. The ICQ, which varies between -0.5 (reflecting exclusion) and 0.5 (perfect colocalization), was close to 0.5 for ab A, while that of ab B was smaller but still positive, a difference with high statistical significance (Table 1; here and elsewhere significance was established through biological replications).

				1		2	3
		N subjects	N, fibers or myotubes	R	ICQ	VS shift, nm	FWHM, µm
JPh44 in myofibers	average	3	10	0.31	0.22	66	0.56
	median			0.26	0.23	54	0.50
	S.E.M.			0.04	0.02	15	0.19
JPh1 in myofibers	average	3	8	0.88	0.4	16	0.42
	median			0.9	0.42	12	0.40
	S.E.M.			0.03	0.02	3	0.07
p				<0.001	<0.001	<0.001	0.06
JPh44 in myotubes	average	2	9	0.37	0.22	168	1.74
	median			0.36	0.22	164	1.69
	S.E.M.			0.05	0.03	36	0.17
JPh1 in myotubes	average	3	29	0.73	0.32	38	0.55
	median			0.77	0.32	38	0.50
	S.E.M.			0.02	0.01	4	0.03
p				<0.001	0.003	<0.001	<0.001

Table 1. Colocalization of JPh1 (as reported by the ab A signal) and its fragment (ab B) with RyR1 in muscle or muscle-derived myotubes. Col. 1: Pearson's pixel-by-pixel correlation coefficient. 2: Van Steensel's shift in the x direction (parallel to fiber axis, arbitrary direction for myotubes). 3: Van Steensel's FWHM of Gaussian fit. 4: Li's Intensity Correlation Quotient. Definitions in Methods. p, probability of no difference between values for JPh44 and JPh1. There was no statistically significant difference between colocalization measures of the same protein in myotubes vs myofibers (p's not shown). *Data trace* : raw data and statistics. In *JPh/manuscript /ColocalizJP44andRyR.JNB*.

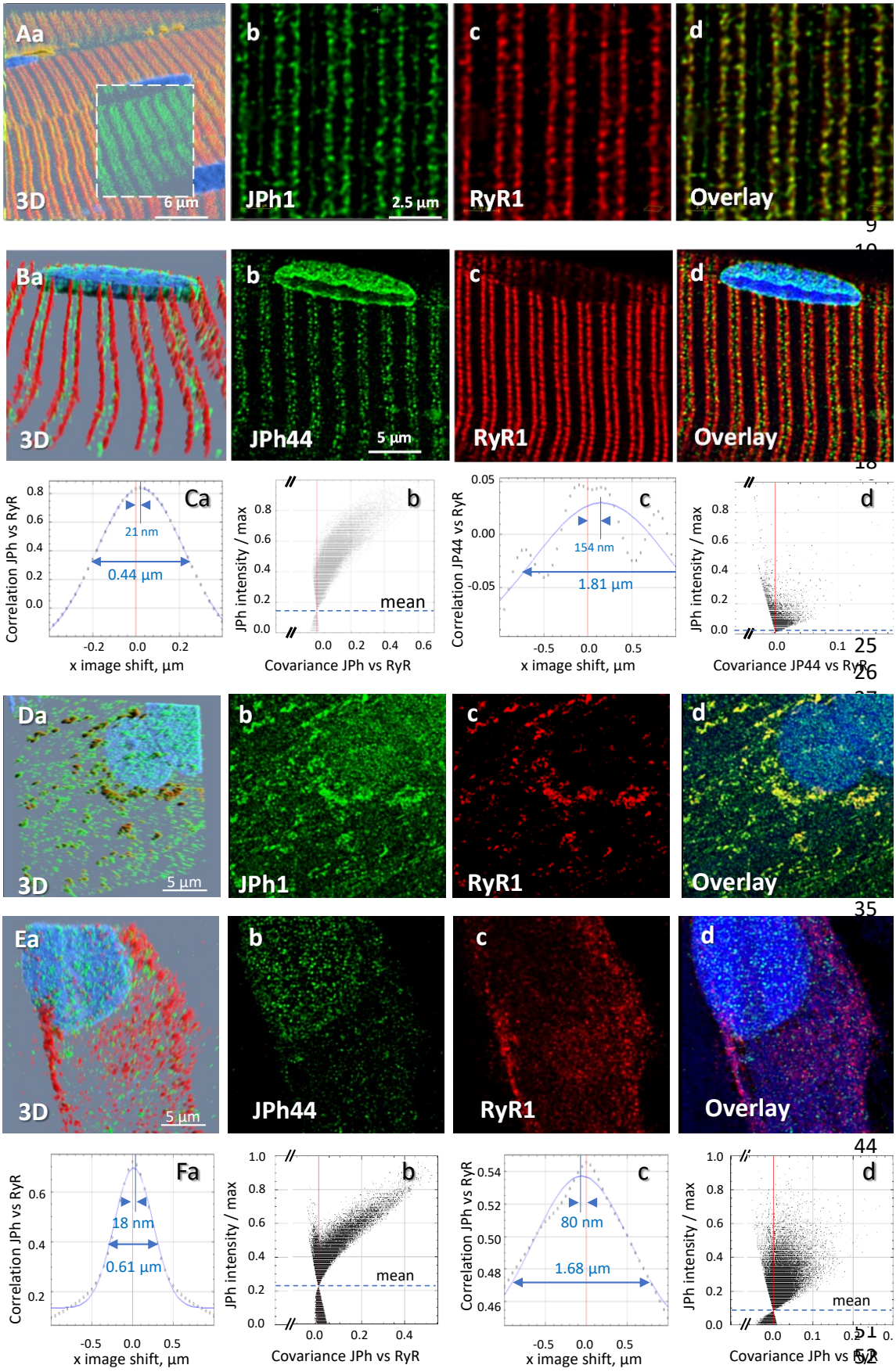

Figure 2. Location of two forms of junctophilin in human skeletal myofibers and myotubes: A, B, Images respectively stained with antibodies A and B, in cells co-stained for RyR1 (Overlay panels add nuclear staining). JPh1 (ab A) and Ryr1 (panels Ab, c) are highly colocalized at T-SR junctions. JPh44 (ab B) moves away into the I band (panels Bb, d). Colocalization between JPh1 and RyR1 is high, as demonstrated by the Van Steensel's and Li's analyses (panels Ca, b), leading to 4 measures (R, VS shift, FWHM and ICQ) listed in Table 1. As indicated in Ca, VS shift is 21 nm and FWHM is 0.44 µm. Colocalization of JPh44 and RyR2 is lost, as indicated by a VS shift of 154 nm, a FWHM of 1.8 µm defined on a Gaussian that fits poorly an oscillating VS plot and a Li plot characteristic of no colocalization and exclusion (compare panels Cb and Cd). D, E, primary myotubes derived from patients' muscle, stained respectively with abs A and B, and co-stained for RyR1. Note in panels D, overlap of JPh1 (ab Al) with cytosolic RyR1. In E, JPh44 (ab B) is largely intra-nuclear, with no colocalization with RyR1. Visual impression is supported by colocalization analyses (panels F, replication results in Table 1). *Data trace*. Average colocalization measures are listed in Table 2. Experiment identifiers: panel A, 102919La Series 010 (ID 167, HH); panel B, 102519L Series 018; panels D, G, 072420Lb Series 002; panel E, 030120Lb Series 001. Data in *Summary ratios.xlsx*.

A third approach, introduced by Van Steensel et al. (37) and illustrated in Fig. 2 panels Ca, c, plots the correlation coefficient of the two signals, averaged over all pixels, vs. a variable shift of one of the images in one direction (in the example, the shift is in the x direction, parallel to the fiber axis). The curve generated is then fitted by a Gaussian. The x-axis location of the apex of the Gaussian (or that of the actual correlation, when the fit is poor), named "VS shift", provides a rough measure of the average separation of the two fluorescent species in the x direction. In the example, the distance was 21 nm for JPh1 (antibody A, panel 2Ca) and 154 nm for JPh44 (2Cc), a significant difference (Table 1). Fourth: the FWHM of the fitted Gaussian is a second measure of dispersion or de-localization, also greater for the JPh fragment. Further use of these techniques will show that the calculation of four different measures provides a multidimensional view of colocalization — or its absence — revealing differences between proteins and treatments not reflected in the usual correlation analysis.

Images of patient-derived primary myotubes, stained with antibodies A and B and co-stained for RyR1, are illustrated in Fig. 2 D, E). Here too, the differences were clear. Ab A staining in cytosol was highly colocalized with RyR1 (2D, 2F, quantification in Table 1), in clusters that presumably correspond to developing junctions. In agreement with the observation in myofibers, ab B did not colocalize with RyR1 and was found mostly within nuclei, in fine granular form (panel 2Eb). Unlike myofibers, myotubes had some intra-nuclear staining with ab A, which adopted a fine granular pattern similar to that of ab B. Observations presented later assign this ab A signal to JPh44.

The 44-kDa fragment internalized in nuclei includes the C terminus of JPh1

Cytosolic/ nuclear density	GFP			FLAG		
	C2C12	Patient-derived myotubes	Murine myofibers	C2C12 myotubes	Patient-derived myotubes	Murine myofibers
avg	2.32	3.13	139	0.84	1.44	0.15
median	2.47	2.62	45.5	0.87	1.4	0.09
sem	0.47	0.59	38.5	0.12	0.26	0.03
N, n, nn	1, 3, 6	1, 4, 38	3, 16, 20	1, 3, 6	1, 4, 38	3, 16, 20
P				0.039	0.028	<0.001

Table 2. Fate of doubly tagged protein GFP (N) – JPh1 – FLAG (C). Distribution of GFP (N terminal) and FLAG (C-terminal) in different preparations, quantified by the ratio of densities in extranuclear ("cytosol") and nuclear areas. N, numbers of culture experiments, patients or mice. n, numbers of images. nn, numbers of nuclei included in calculations. p, probability of no difference between GFP and FLAG distributions in 2-tailed t tests. To correct for data clustering (or pseudoreplication), average and dispersion parameters in mouse myofibers were derived by hierarchical analysis. *Data trace*: Raw data listed in depository under the following identifiers: C2C12: 091620a. Series 2, 5, 7. Patient-derived myotubes: 091020a. Series 1-4. Mice: 092420a, 100520a, 100520b. All series. Murine in *summary flag-gfp.JNB*. Patient in *ColocalizJP44and RyR.JNB* in JPh/Manuscript Data2.

In earlier studies of JPh2, both N-terminal (28) and C-terminal fragments(29) were shown to translocate to nuclei, in conditions of heart stress. To identify the JPh1 segment cleaved as JPh44 and follow its movements, a fusion of JPh1 with GFP (at the N terminus) and the FLAG tag (at the C terminus) was expressed in myotubes derived from patients' muscle or a C2C12 line, and in mouse adult myofibers. Panels A and B in Fig. 3, of myotubes expressing GFP-JPh1-FLAG, show GFP fluorescence (green) largely in the cytosol, in the form of small clusters or puncta. Instead, the C-terminal FLAG (red) appeared in both nuclear and extra-nuclear regions — corresponding to the cytosol and other organelles. The intensity of the intra-nuclear FLAG signal was highly variable in individual nuclei (Supplement Fig. 1 to Fig. 3). Within the cytosol, the FLAG tag was distributed in two forms: punctate, colocalized with (N-terminal) GFP fluorescence, as well as a finely particulate disperse form, away from GFP, obviously corresponding to a fragment cleaved at a position distal to the N terminus.

The asymmetry was quantified by the ratio of signal densities, extra-nuclear (loosely called "cytosolic")/nuclear, which in C2C12 myotubes was approximately 3-fold greater for GFP, a highly significant difference (Table 2). When the plasmid was expressed in myotubes derived from human muscle, a difference greater than 2-fold, again in favor of GFP, was found (panels 3B and Table 2). A clear nuclear internalization of FLAG, with exclusion of GFP, was also found in adult mouse muscle expressing the plasmid (Fig. 3C). In this case the ratio (cytosolic/nuclear) of signal densities was nearly 1000-fold greater for the N-terminal GFP than for the C-terminal FLAG (Table 2).

An additional observation (illustrated with panels 3Ca, d, e and repeated in replications) was that in myofibers of adult mice the C-terminal fragment accumulated in perinuclear regions, in addition to entering nuclei. This was not the case for the native JPh44 in myofibers (Fig. 2), which suggests that the perinuclear buildup be a consequence of the steep gradient generated by the transient increase of concentration of the fragment, combined with a diffusion barrier at the nuclear membrane. The accumulation might also reflect a sequence difference between the exogenous piece and JPh44. This explanation is refuted however, by the absence of perinuclear FLAG accumulation in myotubes expressing the construct (Fig. 3Ad, Bd), which instead suggests a slower production of the protein or a lower barrier to nuclear entry in developing cells.

In the transfected mouse myofibers we also found the N-terminal GFP strictly colocalized with endogenous RyR1 at triads, reproducing the high colocalization of endogenous JPh1 and RyR1 found in human myofibers (illustrated with Fig. 2 and its Supplemental Fig. 1). These observations allow three conclusions: 1) in both developing and adult tissue, the full-size protein is attached to junctions between plasma or T membrane and SR. 2) The C terminus is part of the cleaved fragment that migrates into the I band and enters nuclei. 3) The N terminus of JPh1 stays with the plasma or T membrane, whether as part of the full protein or after cleavage.

Elevated cytosolic calcium concentration mediates the increase in JPh1 cleavage

Resting $[Ca^{2+}]_{cyto}$ in myofibers of MHN and MHS human subjects was reported as 112 nM and 485 nM, respectively (12). Murphy et al. (24) reported some cleavage of JPh1 at $[Ca^{2+}]_{cyto}$ of 500 nm. Hypothesizing that the increased cleavage of JPh1 in MHS subjects is associated with increased $[Ca^{2+}]_{cyto}$, we quantified the effect of this level of cytosolic $[Ca^{2+}]$ on the fragmentation of JPh1. Biopsied myofiber bundles from three subjects, pinned in chambers and exposed to saponin for permeabilization, were superfused with either 100 or 500 nM $[Ca^{2+}]$. After 10 min of exposure, the bundles were processed separately to extract protein (hereon "whole-protein extracts"). Quantitative WB of the extract found increased JPh1 cleavage upon exposure to higher $[Ca^{2+}]$ (Fig. 3 D-F).

Together with an excess JPh44 in whole-protein extracts from MHS patients' muscle, we found a significantly higher JPh44 content in nuclear fractions from these biopsies (Fig. 3G, H). The altered phenotype of MHS patients, including elevated $[Ca^{2+}]_{cyto}$, is reproduced to a large extent in myotubes derived from their muscle biopsies (21,38). Two remarkable observations affirm the relevance of the elevated cytosolic calcium in defining the altered phenotype. First, there was a positive correlation between the nuclear JPh44 content in the muscle of patients and $[Ca^{2+}]_{cyto}$ in their derived myotubes (Fig. 3I). There was also a significant positive correlation between nuclear content of JPh in the myotubes (as quantified by the nuclear/cytosolic ratio of JPh densities) and their $[Ca^{2+}]_{cyto}$ (Fig. 3J). Taken together, the observations indicate that cleavage of JPh1 and nuclear internalization of the 44 kDa fragment are higher in MHS muscle, driven by the higher $[Ca^{2+}]_{cyto}$ found in these patients.

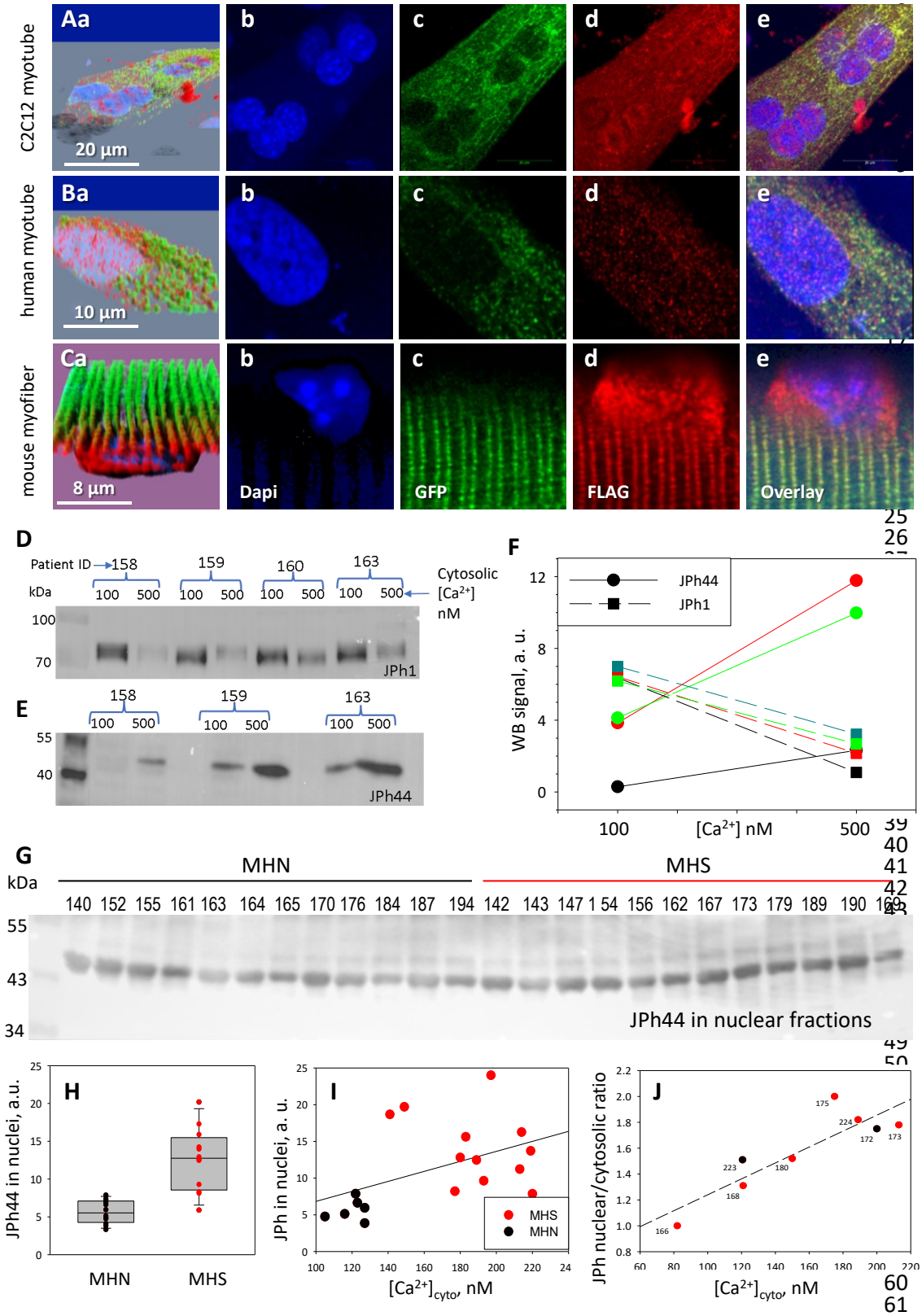

Figure 3. Distribution of a dually tagged JPh1 and its fragments. A-C, confocal images of cells expressing the (N)GFP-JPh1-FLAG(C) construct. In myotubes (A, B), GFP is exclusively in the cytosol, while FLAG, marking the full-size protein and its C-terminal fragment(s), red, distributes widely, including inside nuclei. The different distribution is also evident in adult myofibers (panels C), with the additional observation of accumulation of the N-terminal fragment in perinuclear regions (Cd). Panels Aa, Ba and Ca -- 3D views of the image stacks -- show the intranuclear location of FLAG. Full stacks are viewable as Supp. videos to Fig. 3. The distribution differences are highly significant (details inTable 3). D-F, effect of extracellular Ca^{2+} on JPh1 content of permeabilized muscle from 4 subjects. JPh1 (ab A) and the 44 kDa fragment (ab B) changed reciprocally in muscles exposed to 500 vs 100 nM $[Ca^{2+}]$. G, JPh44 (stained by ab B) in whole muscle nuclear fraction extracted from 12 MHN and 12 MHS individuals. H, the average content is more than 2-fold greater in MHS ($p < 0.001$). I, JPh44 content in nuclei (from WB in panel G) vs. $[Ca^{2+}]_{cyto}$ in primary myotubes from the same muscle samples, showing a statistically significant positive correlation ($R = 0.48$, $p = 0.04$). J, ratio JPh content in nuclei / JPh in cytosol, in images of myotubes stained with ab A, vs. $[Ca^{2+}]_{cyto}$. The correlation is positive and statistically significant ($R = 0.88$, $p = 0.004$). *Data trace*: A: experimental record 091620a Series 5 Lng; B: 091020a Series 4 Lng, from patient MHN #179; C: 100520a Series 2. F, H - J in *JPh vs Ca and GSK3b vs FSB.JNB*. F in Section 1, I in Section 2, J in Section 3.

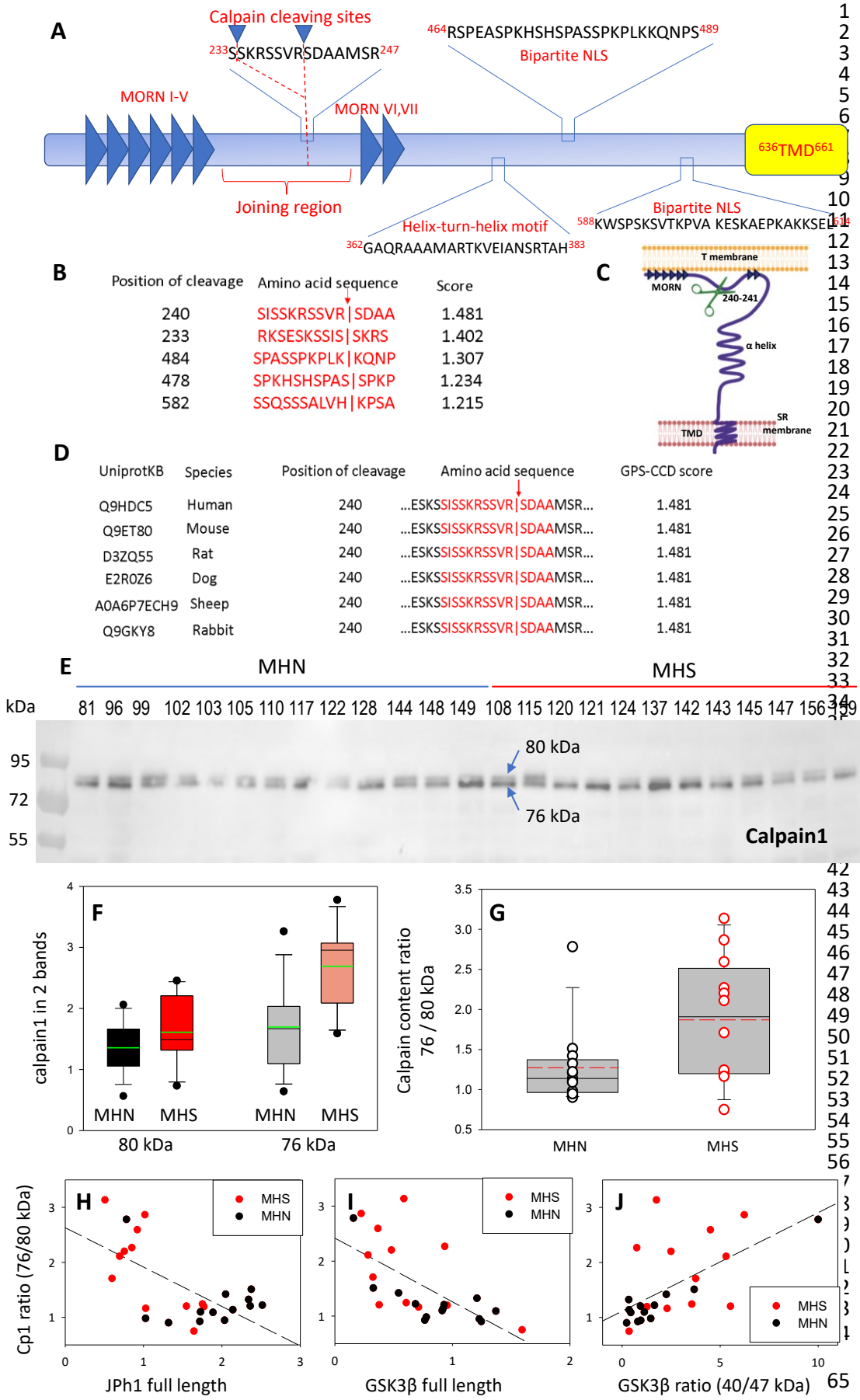

Figure 4. Activation and activity of calpain 1 in muscles of MHS patients. A, JPh1 sequence indicating conserved stretches and the two calpain cleavage sites with highest priority score, located between MORN motifs VI and VII. B, the 5 top-priority cleavage sites predicted by GPS-CCD 1.0 (36). C, JPh1 secondary structure, showing location of the highest priority cleavage site (R240-S241), helix-turn-helix DNA interaction site and TMD in SR junctional membrane. D, conservation of the preferred cleavage sites R240-S241 and S233-S234 in mammalian orthologs, which produce in every case a C-terminal fragment of ~ 44 kDa. E, WB of whole-tissue protein fraction in biopsied muscle of 13 MHN and 12 MHS patients, showing a dual band at ~80 kDa (details in Supplement Fig. 1 to Fig. 4). F, box plot of full-size and 76 kDa truncated forms, compared in the MHN and MHS groups. G, distribution of ratios of 76 /80 kDa forms. Median ratio in MHS (1.97) is 74% greater than that in MHN (1.13) with p = 0.029 of no difference. Automatic quantification of the WB is in Supplement Fig.2 to Fig. 4. H, I, J, correlation of ratios of 76/80 kDa junctophilin 1 with contents of full-length JPh1 and GSK3β, and ratio of activated to full-length forms of GSK3β, derived by WB of the same muscle fractions used for the blot in panel E. The correlation coefficients R and p of no correlation are: for H, -0.65 and <0.001; for I, -064 and <0.001; for J, 0.61 and 0.001. *Data trace*: Panels E-G and H-J respectively in sections 6 and 5 of *Calpain files with correlations ER IDL. JNB.*

Calpain1 cleaves JPh1 to produce a 44 kDa C-terminal fragment

Murphy et al. (24) showed that activation of calpain 1, a heterodimer that incudes a main (~80 kDa) subunit, is associated with autocatalytic proteolysis and results in cleavage of junctophilins 1 and 2. Later studies confirmed that JPh2 in mammalian heart is cleaved by calpains (28,29), most effectively by calpain1 (39), activated upon autolysis to a ~76 kDa isoform (40–42). Because this activation is reported to occur in the 50-300 nM range of $[Ca^{2+}]_{cyto}$, we tested whether calpain1 autolysis occurs and is responsible for the increased cleavage of JPh1 in MHS.

		R	VS shift, nm		FWHM, µm	ICQ	N, subjects n, stacks
			longitudinal	transversal			
JPh1 vs calpain	mean	0.718	31.67	44.67	0.63	0.297	3 9
	median	0.701	28.00	39.00	0.62	0.29	
	sem	0.036	6.41	6.18	0.02	0.012	
JPh44 vs calpain	mean	0.387	66.14	103.86	1.89	0.191	2 7
	median	0.42	60.00	89.00	1.30	0.2	
	sem	0.045	18.19	23.24	0.77	0.028	
	p	*<0.001	*0.151	*0.08	0.02	0.007	

Table 3. Colocalization measures of junctophilin vs calpain in patients' myofibers. p: probabilities in 2-tailed t test or * non-parametric difference of medians. *Data trace*: images of experiments 051220, 113020, 081020 a (JPh1) & 081120b & 120121 (JPh44). *Data trace*: Section 3 in *colocalizationJPhandRyR.JNB*

The prediction tool GPS-CCD 1.0 (43) applied to JPh1 — the human sequence of which (44) is diagrammed in Fig. 4A — revealed several conserved calpain1 cleavage sites in multiple JPh1 orthologs (Fig. 4B). The one with highest score is at R240-S241, within the cytosolic domain, in-between MORN motifs 6 and 7 (Fig. 4A-C). In all these orthologs, cleavage at the R-S site will generate a C-terminal fragment of between 45.92 and 46.28 kDa, consistent with the ~44 kDa migration size of JPh44 and its C-terminal location in the sequence of JPh1.

To test whether the greater cleavage of JPh1 in MHS is due to activation of calpain1 , we analyzed by Western blotting the calpain1 content of muscle from the subjects with JPh content represented in Fig. 1. The immunoblot revealed a double band, with a component at ~80 kDa and another at ~76 kDa, the sizes of the protease and its activated fragment (Fig. 4E). We adapted a custom method to quantify immunoblots (22) to automatically compute the signal in closely placed double bands. Details of the procedure are in supplemental Fig. 1 to Fig. 4. Comparisons of the signal in the two bands between MHS and MHN patients are represented in Fig. 4F. The signal differences between MHS and MHN were not statistically significant for either calpain band. However, the paired ratios of band signals (76 kDa / 80 kDa, Fig. 4G) were on average 74% higher in the MHS ($p = 0.029$). This ratio, which can be taken as a measure of calpain activation, was negatively correlated with both the (72 kDa) JPh1 and GSK3β contents, and positively correlated with content of the 40 kDa GSK3β fragment, quantified in the same muscle samples (Fig. 4 H-J). The relative increase in the 76 kDa fragment was also accompanied by a higher content of smaller polypeptides detected by the calpain1 antibody (supplemental Fig. 2 to Fig. 4).

To test the ability of calpain1 to cleave human JPh1, total protein extracts from patients' muscle were incubated with 0.5 units of calpain1 at different time intervals (Fig. 5A, B). Incubation resulted in cleavage, as reflected in reduction in content of full-length JPh1 and increase of the JPh1 44-kDa fragment (still referred to as "JPh44", even though it was here obtained by a different procedure). The changes were essentially completed in 5 minutes.

The effects of calpain 1 on the two forms were large and reciprocal, and increased with protease concentration (5C, D).

Finally, calpain-dependent JPh1 fragmentation was effectively inhibited in the presence of the calpain inhibitor MDL 28170 (Fig. 5E, F). While the observation is consistent with calpain1-specific cleavage of human JPh1, it does not exclude effects of calpain 2 or cathepsin B, as these are also targets of the inhibitor.

While calpain1 is freely diffusible in the presence of normal cytosolic concentrations of Ca^{2+}, it binds to cellular structures immediately upon elevation of $[Ca^{2+}]_{cyto}$, which implies that its proteolytic activity can only be exerted on substrates that are close-by at the time of activation (45,46). Therefore, to target JPh1 effectively, calpain1 must be present near T-SR junctions. To define this location precisely, human myofibers and human-derived primary myotubes were stained for calpain1, junctophilin (using antibodies A or B), and RyR1 as junction marker, and 3D-imaged at high resolution. Images of endogenous calpain1 in myofibers show that it colocalized with JPh1 (Fig. 5G, Supp. Fig. 1 to Fig. 5) — confirming the presence of the protease near junctions — while JPh44 was found in the I band, not colocalized with calpain1 (5H). The quantitative measures described for colocalization of JPh and RyR1 were also indicative of colocalization of calpain1 with JPh1, but not with JPh44 (Fig. 5 I-K and Table 3).

	With FLAG-calpain	Reference
Average	3.7411	1.1816
Median	3.4118	1.1839
SEM	0.3292	0.0923
p	<0.001	
Subjects, z-stacks	3, 19	4, 18

Table 4. Effect of FLAG-calpain expression on location of JPh1 antibody A (which detects full-size and 44 kDa fragment) in patient-derived myotubes. Location evaluated as ratio of nuclear/cytosolic density of antibody signal. *Data trace*: Section 5 in *colocalizationJPhandRyR.JNB.*

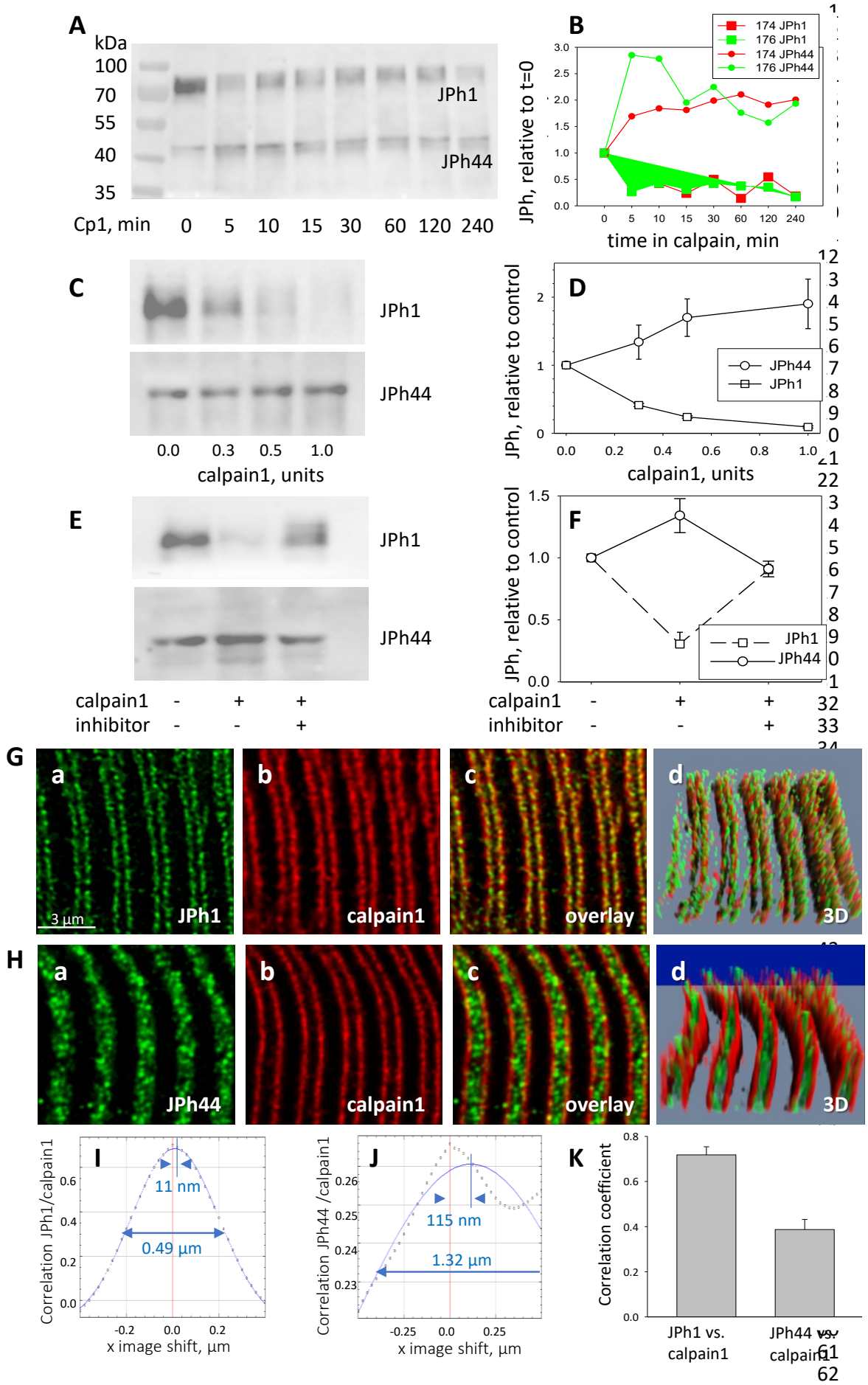

Figure 5. Calpain 1 effects and cellular location. A, B, time dependent changes in content of JPh1 and JPh44 in total protein extracts from patients' muscle, incubated with 0.5 units of calpain1 for different intervals (ab A). B, quantities normalized to initial value. Colors represent different experiments, on tissue from different individuals (2 replicates). C, D, effect of different doses of calpain1 incubated 10 min with the same extract (n = 5 replicates in extracts from 5 subjects). Bars depict SEM. E, F, effect of calpain at 0.5 units for 10 min, with or without MDL28170 (n = 5). In C and E, ab B was used in the JPh44 blot. G, H, confocal images of JPh1 and JPh44 (abs A and B), in muscle co-stained for calpain 1. Gd and Hd are 3D representations of the full z-stack, showing movement of JPh44 away from T-SR junctions (the location of calpain) and into the I band. I, J, Van Steensel's plots show large differences in colocalization parameters VS shift and FWHM, quantifying movement of JPh44 away from calpain. K, correlation between calpain and JPh1 or JPh44 signals. As shown by statistical analysis of replicates in Table 5, the differences in colocalization parameters are highly significant. *Data trace. A, B, and E, F in Calpain files with correlations ER IDL.JNB* (sections 1 and 4). G, H, experiment 081020a Series 5 and 081020b Series2, patient ID #183, MHS. IF images from a MHN subject, to show similar colocalization of JPh1 and calpain, are in Supplemental Fig. 1 to Fig. 5.

Effects of exogenous calpain on living cells

The effects were studied by heterologous expression of tagged calpain1 in patient-derived myotubes. The main effect of the overexpressed calpain1 was an increase in intranuclear localization of JPh (Table 4), illustrated in Fig. 6 with images of a human-derived culture transfected with FLAG-calpain1 and additional comparisons with control cultures in Supplemental Fig. 1 to Fig. 6. Panels 6A-D are 3D renderings of the *z*-stacks of confocal images. A and B show FLAG-calpain1 and junctophilin stained with ab A. Panel C renders RyR1 in the same cells. The images allow direct comparison, within the same field, of a myotube (Cell 1) that expressed strongly the FLAG-tagged calpain1, and one (Cell 2) that had no trace of the protein. Calpain1 (panel A) was widely distributed in the cytosol; nuclei can be recognized in A and C by the absence of calpain1 and RyR1. While the ab A signal (panel B) was widely distributed in Cell 2, in Cell 1 it resided mostly inside nuclei, presumably because it tagged largely JPh44, cleaved by the excess calpain. The intranuclear junctophilin in Cell 1 adopted a diffuse, fine-grained form, while the cytosolic junctophilin in Cell 2 often formed puncta or clusters. The increase in nuclear junctophilin in cells expressing calpain was large and highly significant (Table 5).

RyR1 is clustered in both cells (Fig. 6C, G). The overlay (D) shows that the ab A signal colocalizes with RyR1 (red) in Cell 2, corresponding to the more abundant JPh1 full-size form, but not in calpain-expressing Cell 1, where the signal is largely inside nuclei, presumably marking the JPh44 fragment. As illustrated with Supplemental Fig. 1 to Fig. 6, colocalization of JPh and RyR1 was stronger in control cells (not transfected with FLAG-calpain1), with highly significant differences in all 4 measures (Table 5).

	N, subjects	n, cells		R	VS shift, nm	FWHM, µm	ICQ
Expressing FLAG-Cp1	2	13	avg	0.44	278	3.49	0.22
			median	0.42	130	2.24	0.23
			sem	0.05	127	0.96	0.03
Reference	2	16	avg	0.72	44	0.58	0.30
			median	0.73	48	0.52	0.30
			sem	0.03	5	0.04	0.01
			p*	<0.001	0.008	<0.001	0.023

Table 5. Effect of heterologous calpain on colocalization of JPh (detected with antibody A) and RyR1 in human-derived myotubes. p calculated by Mann-Whitney Rank Sum Test. *Data trace*: Experiments 073020 a (calpain) & b (reference). 010422a (calpain). 010422a (reference). Data in *colocalizationJPhRyR.JNB*, Section #11.

Panels 6E-G show fluorescence in one slice of the *z*-stack, with pairwise overlays in H-J. The calpain1-rich cytosol of Cell 1 shows JPh1 in fine granular form, without clusters (Panel H). The same region shows abundant clusters of RyR1 (6G, I). Cell 2, which lacks exogenous calpain1, shows abundant JPh1 in clusters (F), in almost perfect colocalization with RyR1(panel J), which identifies these puncta as JPh1 in developing T-SR junctions.

In Cell 1, where calpain1 was expressed, the protease was also clustered (panel E), highly colocalized with RyR1, i.e., located at T-SR junctions (panel 6 I, colocalization quantified in Table 6). As argued by Murphy (46), the location of calpain1 at calcium release sites is consistent with the idea that Ca^{2+} activation of calpain1 causes its binding to structures, an effect that places the protease at an ideal location for cleaving JPh1.

Fig. 6 illustrates an additional, frequent observation that we did not pursue further: the cell that expressed the calpain construct (Cell 1) had much greater density of RyR1, consistent with other evidence of a role of the protease in control and promotion of muscle development (e.g. (47)).

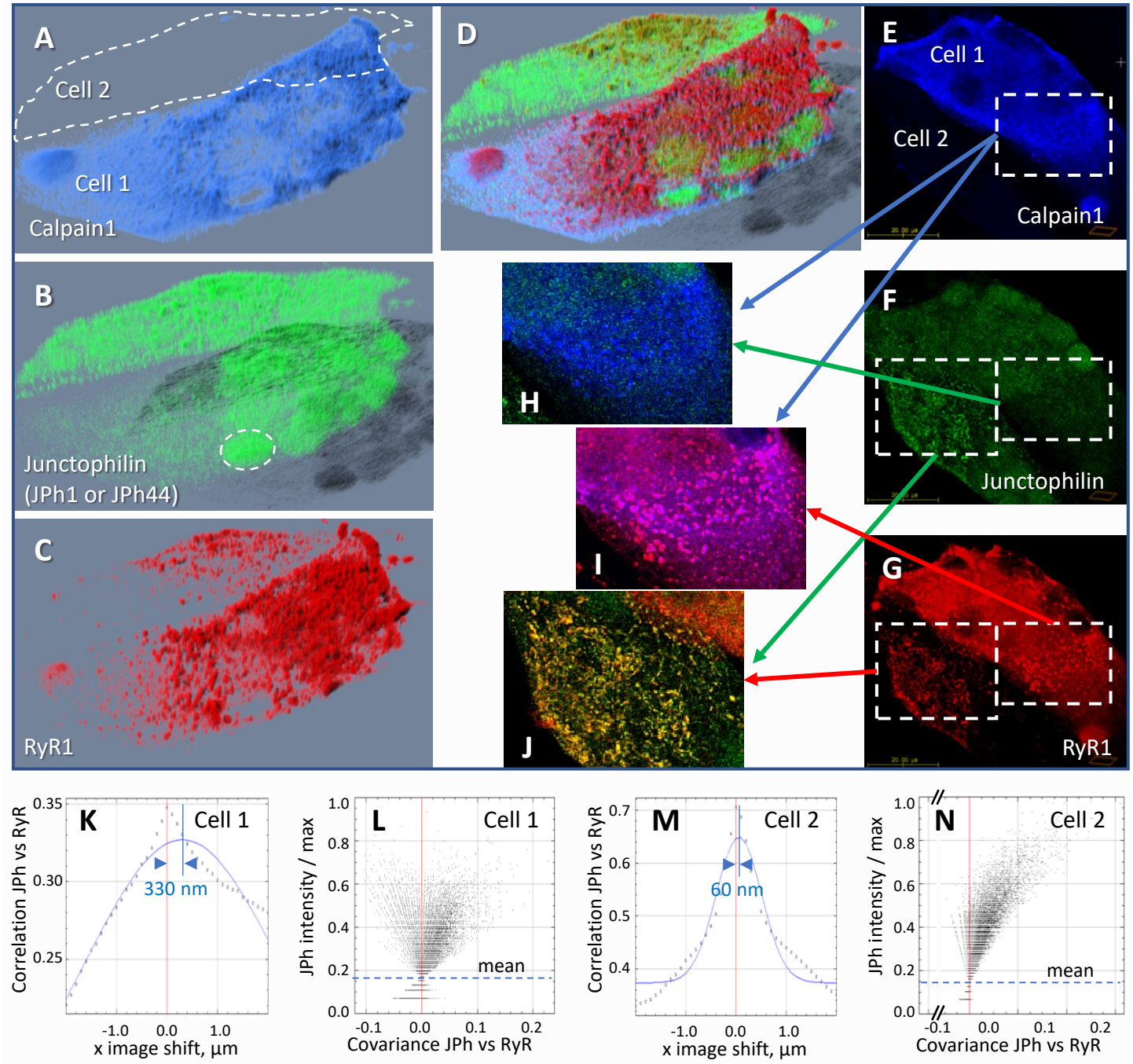

Figure 6. Effect of heterologous expression of calpain 1 on human-derived myotubes. A-D, 3D rendering of a z-stack of images from a culture of primary myotubes transfected with FLAG-calpain 1 (panel A), co-stained for junctophilin with antibody A, which tags both JPh1 and JPh44 (panel B) and RyR1 (panel C). While one of the myotubes (Cell 1) expresses calpain 1 abundantly, the other (Cell 2) does not. In Cell 1, junctophilin adopts a fine-grained appearance and occupies nuclei (e.g., ellipse in B), recognizable by the absence of RyR1 (C, D). In Cell 2 junctophilin is distributed in the cytoplasm, partly colocalized with RyR1. E-G, an individual x-y image (slice) in the z-stack, with sub-sections magnified and superimposed to illustrate colocalization. H, calpain colocalizes poorly with ab A in Cell 1, as junctophilin is largely in cleaved, JPh44 form. I, calpain colocalizes highly with RyR1, forming clusters. J, in Cell 2, which does not express calpain, ab A colocalizes highly with RyR1, indicating full-size JPh1. K-N, Van Steensel's and Li's plots, showing poor colocalization of the junctophilin antibody and RyR1 in Cell 1 (K, L), contrasting with that in Cell 2 (M, N). Statistics of colocalization measures, comparing cultures with and without calpain, are in Table 6. Further evidence of the effect of calpain is provided with Supplemental Fig. 1 to Fig. 6. *Data trace*: Experiment 073020La Series 5. Myotubes derived from patient #180, tested as MHN. Data in *ColocalizJp44andRyR.JNB* sections 5 and 11.

Together, the results reflect calpain1 activation and autolysis in MHS patients by virtue of their elevated $[Ca^{2+}]_{cyto}$, accompanied by localization of the protease at T-SR junctions, where it cleaves JPh1 to produce JPh44. The activated calpain1 also produces the 40 kDa, activated form of GSK3β.

Effects of a JPh1 deletion mutant in mouse muscle and a muscle cell line

The presence of the JPh44 fragment in the nucleus suggested that it plays a role in gene transcription. The calpain algorithm locates the likely cleavage site at between R240 and S241. To test the prediction and produce a stand-in for the JPh44 fragment, we generated the plasmid GFP-Δ(1-240) JPh1, coding for the N-terminal fusion of GFP with the human JPh1 deletion variant that starts at S241, and studied its expression in FDB muscles of adult mice transfected by electroporation. Panels A and B in Fig. 7 compare expression of GFP-JPh1, the full-size construct, with the GFP-tagged deletion variant in myofibers co-stained for RyR1. While GFP-JPh1 remained near RyRs, in triad junctions, the variant moved away, into the I band, in a manner reminiscent of the movement of JPh44 (compare with Fig. 2 A, B). The

Colocalization with RyR1		N, subjects	n, cells	R	VS shift, nm	FWHM, µm	ICQ
JPh	avg	2	10	**0.72**	**44**	**0.58**	**0.30**
	median			0.73	48	0.52	0.30
	sem			0.03	5	0.04	0.03
Cp1	avg	2	14	**0.76**	**126**	**1.13**	**0.34**
	median			0.76	120	0.95	0.36
	sem			0.03	25	0.15	0.03
	p*			0.336	0.01	<0.001	0.206

Table 6. Colocalization of JPh and calpain (Cp1) with RyR1 in human-derived myotubes expressing FLAG calpain. Patient #180 MHN. 073020a. * p calculated by Mann-Whitney Rank Sum Test. *Data trace*: in *ColocalizJP44 and RyR.JNB* section 9. 073020b. 010422a.

movement away from triads (marked by RyR1) was quantified by colocalization metrics (Table 7). Panels 7C and D demonstrate intra-nuclear localization of the deletion variant, reaching concentrations that saturate the light detector at the excitation intensities required to reveal the sarcomeric expression of the protein (e.g., 7C).

The similarity of movements, cellular location and antibody reactivity between the native JPh44 and the exogenous deletion mutant are consistent with a tentative identification of JPh44 as the C-terminal piece of JPh1 with N terminus at S241. The sole alternative sequence consistent with the predictive algorithm, starting at S234, would only differ for having 7 additional residues at the N terminus. Based on this likely identification, we used GFP-JPh1 Δ(1-240) as stand-in to uncover the effects of the native JPh44 fragment on gene transcription and translation.

To this end, GFP Δ(1-240) JPh1 was transfected into C2C12 cells, where its expression was compared with that of GFP-JPh1, using antibodies A and B (Supplement Fig. 1 to Fig. 8). The deletion construct expressed well and could be found inside nuclei (Fig. 8A). Gene expression analysis revealed that, relative to control cells, 121 and 39 genes were respectively repressed or induced ($p < 0.01$) in the transfected myoblasts (Fig. 8B). KEGG pathway-enrichment analysis identified these genes as intimately related to multiple processes, including regulation of the PI3K-Akt-glucose signaling pathway, energy metabolism, muscle growth and lipid metabolism (8C). Specifically, transcription of GSK3β and proteins inhibitory of phosphorylation of Akt/protein kinase B (Pck1 (phosphoenolpyruvate carboxykinase 1, PEPCK-C) (48), RBP4 (retinol-binding protein 4) (49), Repin1 (replication initiator 1) (50), APOC3 (guanidinylated apolipoprotein C3) (51), TRAF3 (TNF receptor-associated factor 3) (52), Ces3a/TGH (carboxylesterase 3A or triacylglycerol hydrolase) (53)) and NGFR (nerve growth factor receptor (54,55)) was inhibited in response to expression of the construct.

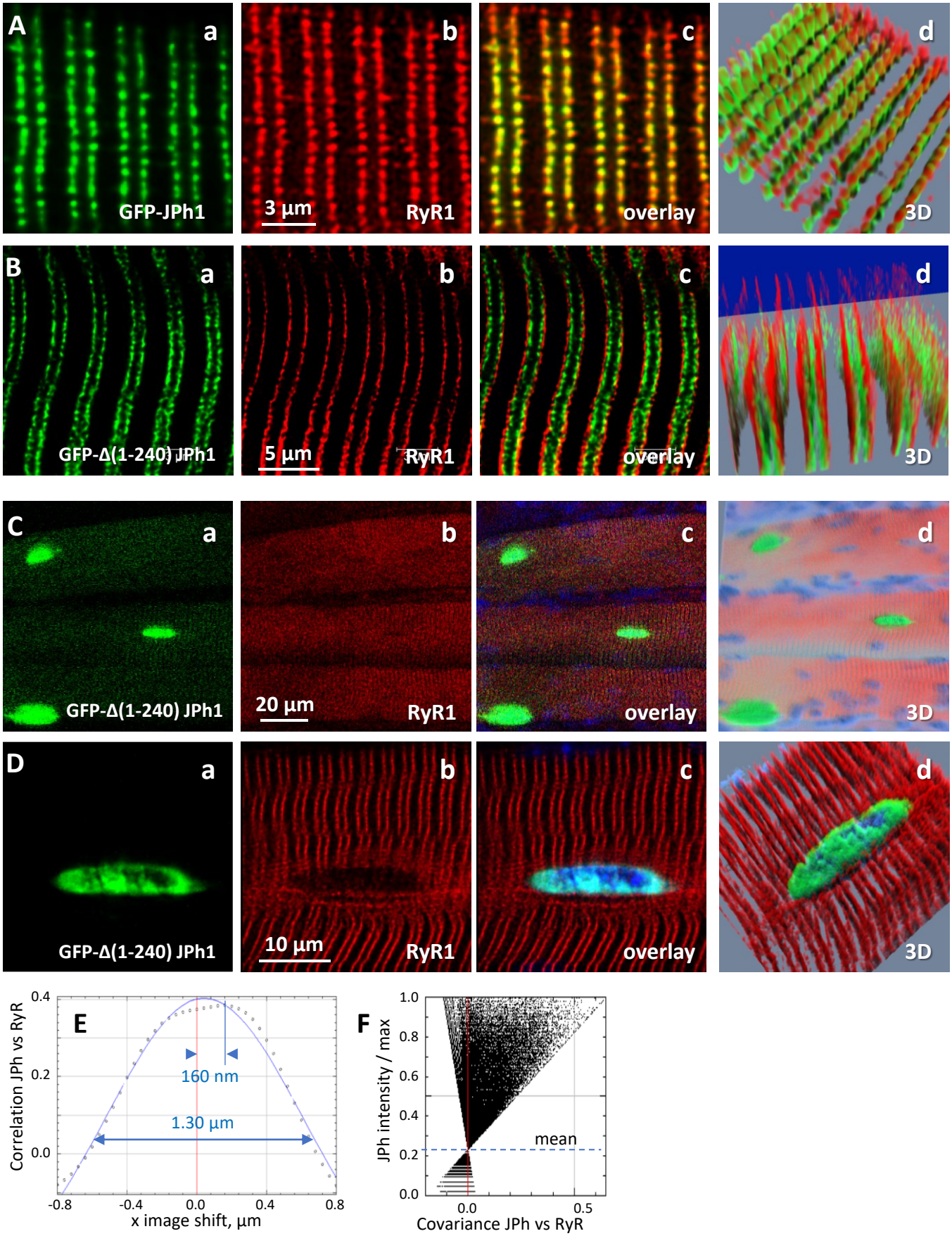

Figure 7. Expression of GFP-Δ(1-240) JPH1 and GFP-JPh1 in adult mouse muscle. A, confocal images of mouse FDB myofibers electroporated with plasmids encoding GFP-tagged, full-length JPh1, co-stained for RyR1. B, mouse FDB myofibers electroporated with plasmids encoding GFP-Δ(1-240) JPh1. C, D, demonstrate the nuclear distribution of the protein upon electroporation of GFP-JPh1 Δ(1-240). E, F, Van Steensel and Li plots, showing absence of colocalization between the exogenous construct and RyR1. Statistics of colocalization measures are in Table 11. *Data trace*: Source files: A, experiment 111220Lb, Series 1. B-D, 110920La, Series 1, 8, 9.

1 These results were validated via qRT-PCR. Consistent with the digital gene expression sequencing analysis, quantification
2 of mRNA content by RT-PCR indicated that the contents of mRNAs for GSK3β, TRAF3, NGFR and Repin1 were
3 significantly reduced by 50% in cells transfected with GFP-Δ(1-240) JPh1 relative to that in control cells transfected with
4 empty vector (Fig. 8D). (Transcription of the other antagonists of Akt phosphorylation listed above could not be
5 evaluated due to failure of all primers tested).
6 As expected from the effects on transcription, we found by Western blot analysis a reduction in GSK3β content in cells
7 transfected with GFP-Δ(1-240) JPh1, by 40% of the content in cells expressing GFP alone (Fig. 8E). The difference was
8 significant (Fig. 8F). By high-resolution imaging we found that cells expressing the JPh deletion construct had reduced
9 levels of GSK3β compared to the neighboring non transfected cells, whereas cells expressing the vector coding for GFP
10 and otherwise empty had similar GSK3β levels to its neighboring cells (Fig. 8Hc and Table 8).
11

		N subjects	n fibers	R	VS shift, nm	FWHM,	ICQ
JPh1	average	3	8	**0.88**	**16**	**0.42**	**0.4**
	median			0.9	12	0.40	0.42
	S.E.M.			0.03	3	0.07	0.02
JPh44	average	3	10	**0.31**	**66**	**0.56**	**0.22**
	median			0.26	54	0.50	0.23
	S.E.M.			0.04	15	0.19	0.02
	p			<0.001	<0.001	0.06	<0.001
GFP-D(1-240) JPh1	average	1	6	**0.54**	**50**	**0.89**	**0.24**
	median			0.53	36	0.80	0.24
	S.E.M.			0.09	23	0.09	0.02
	p			0.001	0.057	<0.001	<0.001

Table 7. Colocalization of exogenous GFP-Δ(1-240) JPh1 with RyR1 in muscle of adult mice. For ease of comparison, the table includes values of JPh1 and JPh44 in human muscle, from Table 1. Bottom row: p of no difference between values for fragments vs. JPh1 (Mann Whitney Rank Sum for all but ICQ). *Data trace*: in *ColocalizJP44andRyR.JNB*

	1	2	3	4	5	6
GSK3β density, a. u.	Cells expressing Δ construct	Cells not expressing Δ construct	Ratio col1/col2	Cells expressing GFP-EV	Cells not expressing GFP-EV	Ratio col4/col5
avg	441	729	0.62	1548	1553	1.00
median	353	547	0.61	1513	1355	1.03
sem	75.1	138	0.03	268	281	0.05
N, images	10	10	10	8	8	8
n, cells	15	73		11	42	
p			<0.001			0.958

Table 8. Effect of expression of GFP-Δ(1-240) JPh1 (Δ construct) on density of GSK3β in C2C12 myoblasts. The reference, in Cols 4-6, is a culture transfected with the empty vector (GFP-EV). The numbers are averages of densities and their ratios calculated individually for 10 and 8 images, respectively for Δ construct and empty vector. The number of expressing cells per image varied between 1 and 3; that of non-expressing cells between 6 and 10. p is the probability of a ratio of 1, i.e., no effect of the expression, based on a 2-tailed t-test on the sample of 10 or 8 ratios. An alternative t-test (of paired differences in density between non-expressing and expressing areas) yielded a p of no difference = 0.002 and 0.930 respectively for the Δ construct and the empty vector. *Data trace*: in *GSK3B graphs and statistics.JNB*

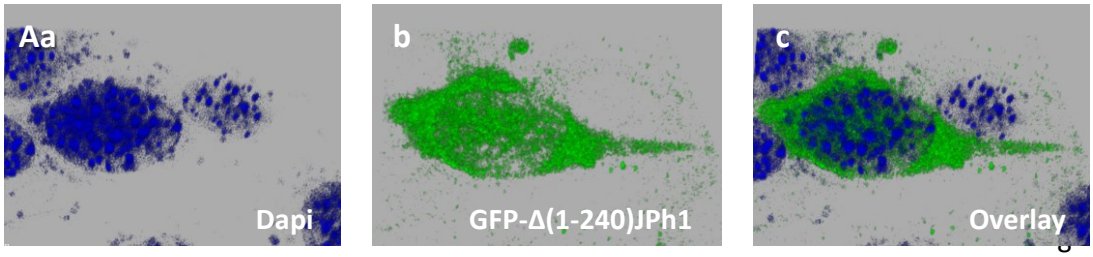

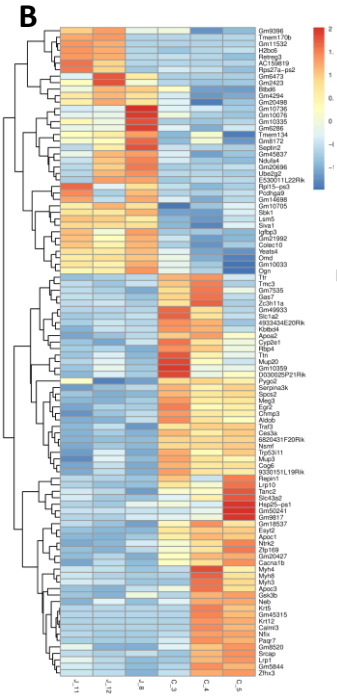

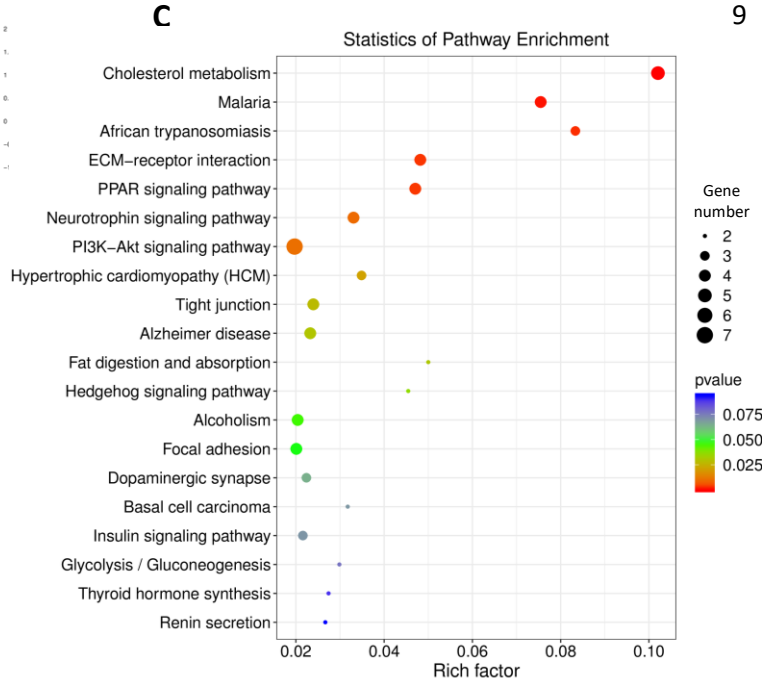

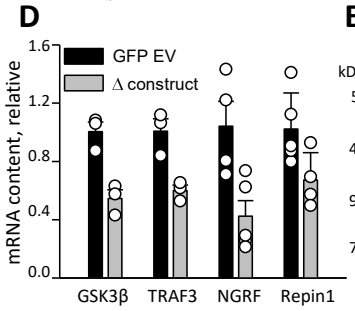

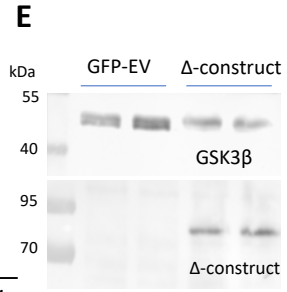

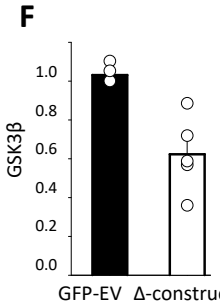

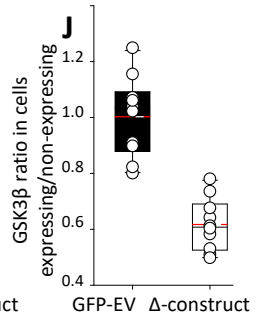

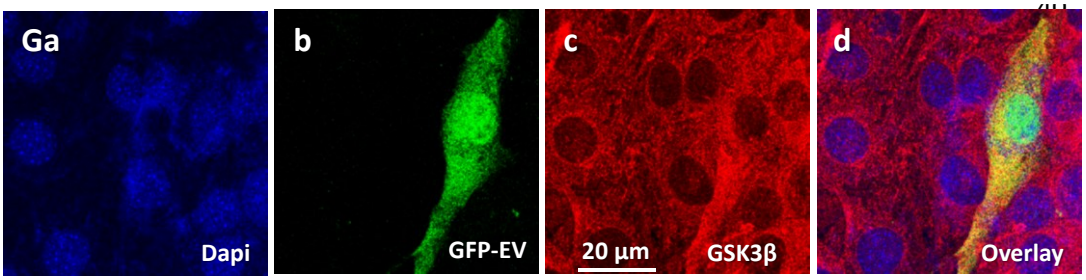

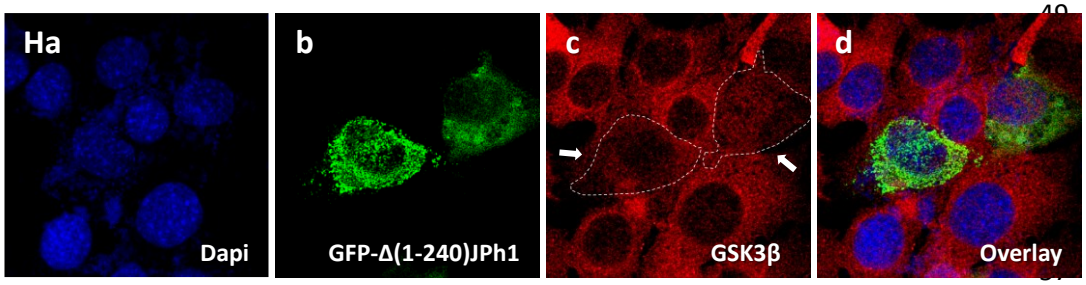

Figure 8. Regulation of transcription in C2C12 myoblasts. A, confocal images of cells transfected with GFP-Δ(1-240) JPh1 vector ("Δ-construct") showing the expressed protein inside nucleus. B, heat map of significantly altered genes in myoblasts expressing GFP-empty vector or Δ-construct. C, KEGG pathway enrichment analysis of transcripts significantly altered by the construct (analysis by LC Sciences, Houston, TX, USA). D, validation of 4 results in B by PCR in our laboratory. Samples from cultures transfected with Δ-construct. Significant differences for GSK3β, p = 0.007; TRAF3, p = 0.012; NGRF, p = 0.015. For Repin1, p = 0.053. E, Western blot of GSK3β in total cell extracts from cells expressing GFP-empty vector or Δ construct. F, GSK3β protein signal in WB of panel E. G, confocal image of GSk3β immuno-fluorescence (red), in C2C12 cells transfected with GFP-empty vector, to compare cells that expressed the marker (green) with those that did not. H, image for similar comparison of GSK3β content in cultures transfected with Δ construct, showing deficit of GSK3β in expressing cells (green). J, comparison of ratios of GSK3 β signal in cells showing the GFP tag over those not expressing it. Statistics in Table 10 shows high significance of the difference. *Data trace*. Source files: A, 110121La series 003. B, C, gene expression profiling data in Dropbox / JPh / manuscript / F9 panels. D, in D:/Jph/ manuscript /f9 panels/ *qPCR.JNB*. E, uncropped blots and gels in raw western blots and gels.doc. F, in *GSK3B levels.JNB* in D:/JPh /manuscript/ F9 panels. G, 102921La series9. H, 110321 Lb series7. J, D:/Jph/manuscript/Fig 1/*GSK3B graphs and statistics.JNB*, section 4.

Discussion

Starting from the observation of reciprocal differences in content of the structural protein JPh1 and its fragment JPh44 in muscle of patients with chronically elevated cytosolic Ca^{2+}, we here identified the pathogenic mechanism leading to these differences. We also demonstrated gene regulatory roles of JPh44, potentially compensatory of the pathogenic consequences of the elevated $[Ca^{2+}]_{cyto}$.

Junctophilin1, calpain1 and the kinase of glycogen synthase undergo fragmentation in MHS patients

Junctophilin (5) is one of the 5 proteins deemed essential for functional, skeletal-muscle-style calcium signaling for EC coupling. We now show that a 72-kDa form of JPh1 (the top size detected in our samples) was reduced by ~50% in total protein extracts of muscles of MHS patients (Fig. 1A, C). A 44-kDa fragment increased in the same patients, albeit in a lesser proportion, a discrepancy that we attribute to proteolysis at other sites in the full-length molecule (Fig. 1B, D, E).

These changes join a wide-ranging pathogenic alteration of cellular metabolism in these patients, which comprises changes in content, distribution and posttranslational modification of multiple proteins. The observed modification of multiple molecular players of glucose utilization by muscle is the likely cause of the hyperglycemia and diabetes that disproportionally affects MHS patients (22,23). Here we demonstrate a conversion of the original ~47-kDa GSK3β molecule to a ~40 kDa form, a truncation that activates the enzyme (33–35). Muscle-specific ablation of this protein inhibits glycogen synthase in mice, improving glucose tolerance, correlated with enhanced insulin-stimulated glycogen synthase activation and glycogen deposition (56). Therefore, we surmise that the activation of GSK3β found in these patients constitutes an additional link in the pathogenic chain that leads from increased $[Ca^{2+}]_{cyto}$ to alteration in muscle utilization of glucose, then to hyperglycemia and diabetes (22,23,57).

The present study used techniques for imaging protein localization that, as documented in our earlier work (22), reached a spatial resolution beyond the theoretical optical limit, unprecedented in studies of live muscle. From this vantage point, we demonstrated consequences of cleavage of junctophilin1. While the full-size molecule is located at T-SR junctions (as demonstrated by quantitative measures of colocalization with RyR1; Fig. 2 A, C, and Table 1), the fragment JPh44 leaves the junctions and migrates into the I band (Fig. 2B, C, and Table1).

The fate of JPh44 was further followed on primary myotubes derived from patients' muscle, where it was seen to migrate inside nuclei (Fig. 2E, F). By contrast, JPh1 remained outside, largely in clusters corresponding to developing T-SR junctions, as revealed by high colocalization with RyR1 (Fig. 2Dd, Fa, b and Table 1). To define the primary sequence of JPh44, the construct (N)GFP-JPh1-FLAG(C) was expressed in myotubes and adult mouse muscle. The consistent presence of the FLAG tag inside nuclei (Fig. 3A-C and Table 2) plus the persistence of the N-terminal GFP in the cytosol, forming clusters analogous to those of JPh1 and RyR1 (Fig. 2) in myotubes, and staying aligned with junctional triads in myofibers (Fig. 3C), unambiguously indicate that the doubly-tagged exogenous protein undergoes cleavage similar to the endogenous JPh1, and that the cleaved fraction that enters nuclei -- corresponding to JPh44 -- includes the C terminus of JPh1. The persistence of GFP outside nuclei indicates that the N-terminal fragment cleaved from JPh1 conserves at least some of the features, presumably the MORN motifs, by which JPh1 attaches to T tubule and plasma membranes (7). However, the stable location of the N-terminal cleavage fragment of JPh1 at triad junctions is inconsistent with the proposal that assigns the specific triadic location of JPh1 to its ability to dimerize (7), as this ability is likely lost in the N-terminal fragment.

$[Ca^{2+}]_{cyto}$ determines JPh1 fragmentation and relocation

Direct perfusion of permeabilized human myofiber bundles with elevated Ca^{2+} concentrations resulted in reciprocal changes in JPh1 and JPh44 content (Fig. 3D-F). While the application of Ca^{2+} was only transient, the major, statistically significant changes that resulted are consistent with a causative involvement of the chronically elevated $[Ca^{2+}]_{cyto}$ in the pathogenic process that takes place in MHS muscle. This process included a large increase in JPh44 content in blots of the nuclear fraction extracted from MHS patients muscle (Fig. 3G, H), which positively correlated with the $[Ca^{2+}]_{cyto}$ measured in myotubes derived from the same patients (Fig. 3 I). This correlation linked a feature of adult muscle with a measure in the derived culture, and notably also applied to JPh localization in patients' myotubes relative to their $[Ca^{2+}]_{cyto}$ values (Fig. 3J and supplemental videos to Fig. 3).

Probable identification of the cleavage site in junctophilin1

The identification of elevated $[Ca^{2+}]_{cyto}$ as mediator of the MHS cellular phenotype pointed at the Ca^{2+}-activated calpains as enzymatic agents of JPh proteolysis. An algorithm predictive of calpain cleavage sites within protein sequences (43) contributed evidence of involvement of calpain1. Among the predicted cleavage sites in JPh1 (Fig. 4B), the one with the highest score, at R240-S241, is highly conserved in mammals (Fig. 4C), producing in every ortholog a C-terminal fragment of approximately 46 kDa. This exercise proposes JPh44 as the C-terminal fragment of JPh1 with N terminus at S241. The cleavage site S233-S234, also of high probability score, suggests an alternative sequence, identical except for 7 additional aminoacid residues at the N terminus. The extra residues would neither cause a difference in molecular weight detectable by electrophoresis nor be likely to change other physicochemical properties, including putative gene regulatory functions suggested by the nuclear localization. Both cleavage sites predict an N-terminal fragment that contains 6 MORN motifs, a prediction consistent with the observation that the N-terminal fragment of JPh1 stays at T-SR junctions (Fig. 3). Recent cryo-EM evidence of the tertiary structure of JPh isoforms 1 and 2 (44) contradicts the conventional view of the helical backbone as spanning the inter-membrane gap (26), suggesting instead a detailed, presumably tight association of this region with the β sheet formed by the MORNs. If this were the case, a single cut at either site might not be sufficient to allow separation of the distal fragment, suggesting instead that both cuts might be necessary to free JPh44.

A key aspect of this process is the link between elevated $[Ca^{2+}]_{cyto}$ and activation of calpain to directly cleave JPh1. The link was first described in skeletal muscle, starting from the notion that acutely elevated $[Ca^{2+}]_{cyto}$ impairs EC coupling (58,59), followed by the demonstration of calpain activation and junctophilin proteolysis at Ca^{2+} concentrations in a range ≥ 500 nM (24,60). Activation of calpain1 requires only moderate elevation of $[Ca^{2+}]$ (50-300 nM) and includes autolysis of its main subunit, which removes an N-terminal piece to bring the molecular weight from 80 to 76 kDa (40–42). We found that in MHS muscle, the fraction of calpain1 in 76 kDa form is about 80% higher than in controls (Fig. 4D, F). That this piece represents activated protease was affirmed by the high negative correlation between the drop in JPh1 content and the fraction of truncated protease in MHS muscle (Fig. 4H). A negative correlation of similar significance between calpain truncation and content of the full length GSK3β is evidence of an additional role of calpain1, namely proteolysis and activation of the GS kinase (Fig. 4 I).

In agreement with the calpain1 predictive algorithm, the protease cleaved the JPh1 protein extracted from human muscle *in vitro,* in a time- and concentration-dependent manner, to a form with the same apparent molecular weight of the native fragment we call JPh44, an action suppressed by a calpain inhibitor (Fig. 5).

Additional evidence linking calpain activation to JPh1 cleavage was obtained by its expression in human myotubes. As illustrated in Fig. 6, heterologous expressed calpain caused a visible increase of JPh44 — distinct from the full-size protein for adopting a fine-grained appearance— which moved massively into nuclei (Cell 1 of panels 6B and D, Table 4; see also Supplemental Fig. 1 to Fig. 6). Concomitantly, the colocalization of JPh and RyR1 was diminished (Table 5). Also consistent with cleavage of JPh1 by the heterologous calpain1 is the high colocalization of the two molecules, contrasting with the low colocalization of JPh44 and the protease (Table 3).

Previous studies reported that calpains cleave couplon proteins, including RyR1 (61) and STAC3 (62). The present findings show that the protease is at the right location for those actions. Both endogenous calpain1, imaged by immunofluorescence in human muscle (Fig. 5G and Supplemental Fig.1 to Fig. 5), and FLAG-tagged calpain1 (Fig. 6 I) were found precisely located at triad junctions; the location was confirmed by its high colocalization scores with JPh1 and with RyR1 (Tables 3 and 6). The observations support the proposal that the protease is freely diffusible in apo form but binds to cellular structures immediately upon exposure to high [Ca^{2+}] (37). Indeed, the quantitative measures of colocalization with RyR1, especially the spatial shift and Gaussian spread obtained with the Van Steensel method, show that the junctional protein JPh1 has a tighter overlap with RyR1 than calpain1 (Table 6), which suggests the coexistence of bound and diffusible forms of the protease.

From Ca^{2+} dysregulation to hyperglycemia and diabetes

The results reviewed above establish with a high degree of confidence that the reduction in JPh1 content observed in MHS patients is caused by calpain1, activated by excess cytosolic calcium, and that the activated calpain also cleaves the specific kinase of glycogen synthase GSK3β, with inhibitory consequences on glycogen synthesis. This effect, together with the putative cleavage of the regulated glucose transporter GLUT4 (63), impair glucose utilization by muscle.

In 2019, Altamirano et al. (23) first called attention to the high incidence of hyperglycemia and diabetes developing in patients years after they were diagnosed with MHS. Aware that the main proximate cause of insulin resistance and hyperglycemia is failure of glucose processing by muscle (e.g., (57)), we set out to understand the pathogenic pathway linking MHS and diabetes. The question is relevant beyond the MHS syndrome, as a similar dysregulation of Ca^{2+} homeostasis is found in other conditions, including related inheritable diseases with mutations in couplon proteins (9,64,65), DMD (17–19), Exertional and Non-Exertional Heat Stroke (66,67) and Statin-related Myotoxicity (68). We found a wide-ranging alteration of location and phosphorylation of the enzymes that manage storage of glucose as glycogen in muscle, namely glycogen synthase, glycogen phosphorylase and their controlling kinase PhK (69), leading to a shift of the glucose ←→ glycogen balance towards glycogenolysis(22). Additionally, we found a decrease in the deployment (translocation) of GLUT4 (22).

The present study adds two nested mechanisms (schematically represented in Fig. 9 together with those previously revealed by (22)), which operate in the same direction: first, the activation by Ca^{2+} and autolysis of calpain1 (Fig. 4D-F). Because calpain1 is known to lyse GLUT4 and increase its turnover (63), its activation is a likely explanation for the observed decrease in translocation of the transporter (22). The second link to diabetes is the observed activation, again by proteolysis mediated by the activated calpain, of GSK3β (Figs. 1F-I and 4H, I). The activated kinase would add its inhibitory effect on GS to that of phosphorylation by the activated PhK (22).

The link between the high activity of GSK3β and diabetes in human skeletal muscle is well established (70), as is the therapeutic potential of GSK3β inhibitors (71,72). It is manifested in our patients by the correlation observed between

content of activated kinase and FBS (supplemental Fig. 4 to Fig. 1). Regulation of GSk3β activity by proteolysis was first reported in the brain, where it was found associated with Tau hyperphosphorylation in Alzheimer's disease (33); the present study provides the first demonstration of its occurrence in skeletal muscle, where it leads to phosphorylation of glycogen synthase, as indicated by the correlation found between GSK3β cleavage and blood sugar.

Taken together, the present observations and those in (22) identify a multi-lane pathway, where Ca^{2+} activation, proteolysis and phosphorylation, involving at a minimum calpain 1, GSK3β, GS, GP, PhK and GLUT4, lead from the primary Ca^{2+} dysregulation to hyperthermia and diabetes (Fig. 9).

The Ca^{2+}-promoted cleavage of junctophilin1 produces an adaptive transcription regulator

Calpains 1 and 2 activate in heart muscle damaged by ischemia (e.g., (73,74)) or in conditions of heart failure, to proteolyze JPh2 (24,29,75). The lysis of JPh2 is associated with structural remodeling, loss of dyadic junctions and deficit of EC coupling function, all expected from the breakage of a structural brace of the junction (76). Surprisingly, however, L-S Song's group went on to demonstrate that a large N-terminal calpain1-cleaved fragment of JPh2, named JPH2-NTP, enters nuclei, where it regulates transcription of multiple genes, with consequences that oppose the damaging effects of activated proteases (28). In contrast, Lahiri et al. (29) reported the presence of a ~25 kDa C-terminal product of cleavage by calpain2, which was shown to be causative of cellular hypertrophy, rather than compensatory.

The present observations establish similarities and differences between the roles of JPh44 and those of the fragments described in cardiac muscle. The distribution of exogenous doubly tagged JPh1 and its fragments (Fig. 3A, C and Table 2) establishes that JPh44 is a C-terminal fragment. The calpain predictive algorithm, together with the observed distribution of the GFP-tagged Δ(1-240) JPh1, also establish with high likelihood the site of JPh1 cleavage, at either R240-S241 or S233-S234 (Fig. 4A). In addition to matching the apparent molecular weight of the endogenous JPh44, the C-terminal fragment resulting from cleavage at either point contains two nuclear location sequences, allowing nuclear import of the fragment (Fig. 4A). Like JPH2-NTP, the fragment will have an alanine-rich region (ARR), with helix-turn-helix (HTH) structure, characteristic of DNA-binding proteins. These properties establish with reasonable likelihood the primary structure of JPh44 as the C-terminal fragment of JPh1 that starts at S241 or S234. We used this identification to probe directly the possible roles of JPh44. in adult mice muscle and C2C12 myoblasts. When expressed in muscle of adult mice, the GFP-tagged Δ(1-240) JPh1 appeared located similarly as JPh44 in human muscle, largely within the I band and inside nuclei, eschewing triadic junctions and colocalization with its marker, RyR1 (Fig. 7B-D and Table 1).

In C2C12 myoblasts, the construct likewise distributed inside nuclei, as well as in a fine-grained cytosolic form (Fig. 8A and Supplemental Fig. 1 to Fig. 8). Consistent with a gene regulatory role of JPh44, the transcription profile (obtained by LC Sciences) of myoblasts expressing GFP-tagged Δ(1-240) JPh1 showed significant alterations in multiple pathways (8B, C). Notably, the profile included significantly reduced mRNA levels of GSK3β and at least 9 proteins that act as brakes on the PI3k-AKT pathway, among which TRAF3, Ces3a (53), Repin1(50) and Pck1 (48) stand out, given their role in muscle metabolism. By quantitative PCR we confirmed the substantial reduction in transcription of four of those genes, as represented schematically in Fig. 9.

The many signaling pathways regulated by Akt importantly include glucose uptake by muscle and adipocytes. In muscle, Akt isoform 2 is activated via phosphorylation by a chain of events at the plasma membrane, started in response to insulin (77); this activation promotes translocation of GLUT4 to the membrane, enabling its transport role. Phosphorylation by Akt also inactivates GSK3β, which in turn releases glycogen synthase from inactivation, promoting

storage of glucose. Hepatic and skeletal muscle silencing of the four genes named above improved the insulin resistance by inducing phosphorylation of Akt (48,50,52,53,78). Other genes repressed by the exogenous JPh1 fragment JPh44, including Rbp4 (retinol-binding protein 4), Apoc3 (apolipoprotein C-III), MEG3 (maternally expressed gene 3 — a long noncoding RNA) and NGFR contribute to insulin resistance by various actions in other tissues (49,51,54,79). Together, the effects on transcription of the exogenous JPh1 fragment are consistent with a beneficial, "stress-adaptive" role of the endogenous JPh44, similar to that ascribed to JPH2-NTP in stressed myocardium (28).

In spite of the similarity, there are many differences between the putatively regulatory fragments of the two junctophilin isoforms. Unlike JPH2-NTP, JPh44 loses an N-terminal portion and with it the main stretch of MORN motifs. If the helical backbone were tightly bound to the MORN β sheet, as argued in (44), separation from the N-terminal fragment that includes most MORNs would free the helix for its putative interactions with DNA inside nuclei. Unlike JPH2-NTP, JPh44 retains a second NLS (K588-L614, Fig. 4A). Therefore, the skeletal muscle fragment appears to have advantages over JPH2-NTP, to leave the junctional location (by losing most T-membrane anchors), and to reach inside nuclei, by having an additional NLS.

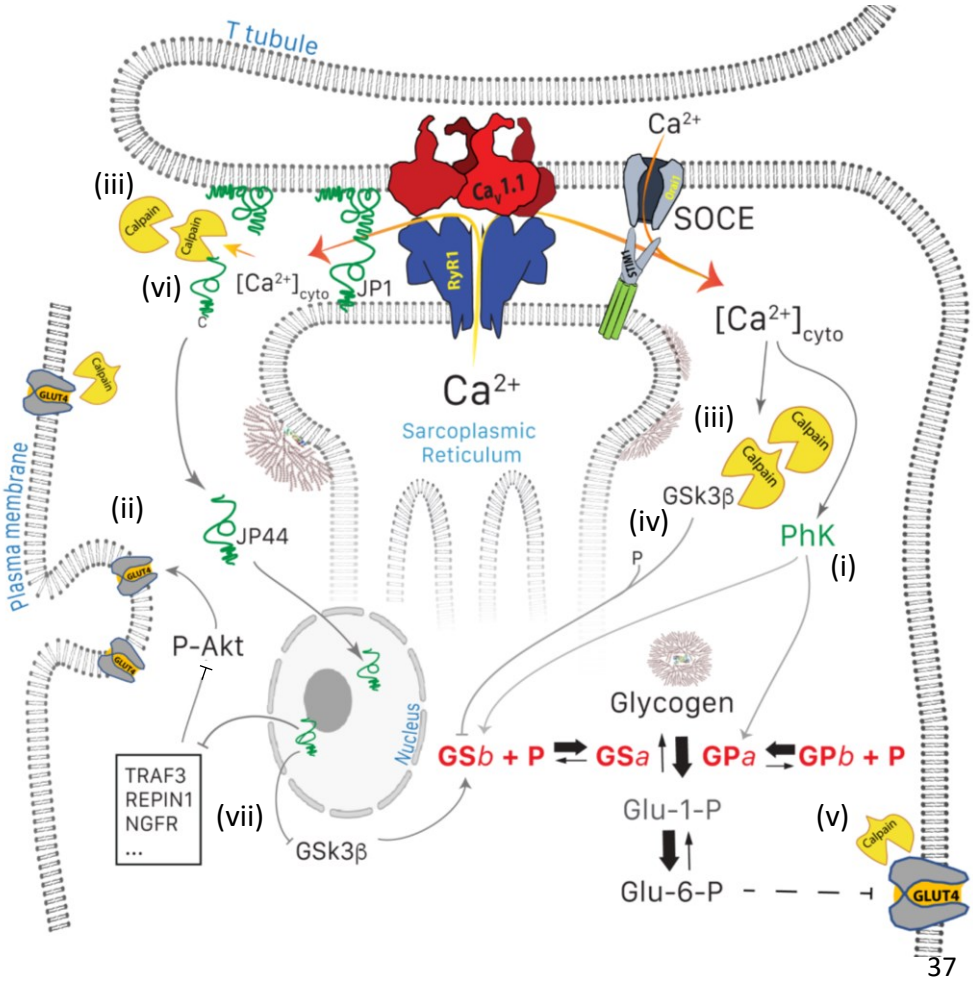

Fig. 9. Glucose pathways of muscle and their alterations under calcium stress. Glycogen, resident in the intermyofibrillar space in the form of granules or SR-bound, is synthesized from transported glucose or broken down to glucose-1-phosphate (Glc-1-P). Sustained elevation of $[Ca^{2+}]_{cyto}$ induces multiple changes: (i) PhK is activated, which increases phosphorylation of GP and GS, to respectively enhance the breakdown and decrease the synthesis of glycogen. (ii) Expression and membrane insertion of the glucose transporter GLUT4 decrease (61). (i) and (ii) contribute to reducing glucose utilization. To these effects, established by (22), the present study adds five mechanisms: (iii), activation of calpain1, associated with autolysis; (iv) cleavage of GSK3β, which activates the kinase to phosphorylate and thereby inhibit GS; (v) lysis of GLUT4, which together with (iv) depress glucose utilization further, and (vi), cleavage of JPh1 to JPh44, which enters nuclei to modulate expression of multiple genes (vii). Mechanisms (i) to (v) contribute to the disease phenotype. While cleavage of JPh (vi) should be deleterious to structural stability, the downstream effects of JPh44 are predictive of beneficial consequences, adaptive to the condition of stress.

Limitations

The degree of autolysis of calpain in the samples that we analyzed is substantially greater than that reported for muscle tissue processed immediately after excision (24,80,81). This fact indicates protein degradation in the human samples after excision, and is consistent with the difference in gel migration between our mouse and human samples (Supp. Fig. 1 to Fig.1). While these indications introduce some uncertainty about the molecular sequence of the JPh fragments of interest, they do not preclude the comparisons between human samples, as they are all treated in the same manner.

Ideas and Speculations

An additional difference between the MHS condition and the stress of heart failure reported to unleash calpain cleavage of JPh2 is that the cardiac condition is accompanied by structural remodeling with loss of couplons and reduction in JPh2 content (76,82), while no structural remodeling has been reported in muscle of MHS patients. Moreover, studies of Ca^{2+} release function revealed an increase in muscle sensitivity to stimuli (membrane voltage or calcium, e.g., (21,38)) rather than the major deficits expected to arise from a loss of functional junctions (3) upon JPh1 loss in the proportion observed here.

A speculative explanation recalls the expression of both JPh1 and 2 in skeletal muscle, both capable of sustaining calcium release function (83). The presence of two molecules that share a function — a redundancy of paralogs — would combine with a different level of redundancy, the presence of multiple copies of the same protein, perhaps polymerized (7), to provide a “sentinel” role. When proteolysis is activated in pathophysiological situations, limited JPh1 cleavage would cause minimal or no deterioration of structure or function, while producing an adaptive gene-regulatory messenger.

Conclusion

We report that the elevated $[Ca^{2+}]_{cyto}$ in skeletal muscle of individuals with MHS activates calpain1, which associates to T-SR junctions. The protease then cleaves a kinase that inhibits glycogen synthase, an effect that correlates with and probably contributes to an increase in blood glucose concentration. Cleavage of the kinase and that of GLUT4 promote the transition to hyperglycemia and diabetes found in many of these patients. It also cleaves junctophilin1, to produce a C-terminal fragment of ~44 kDa that abandons junctions and enters nuclei. There, the fragment modulates transcription of multiple genes, resulting in effects opposing the deleterious alteration of the glucose utilization pathway. Borrowing a term applied to a fragment of junctophilin2 found to enter nuclei in myocytes of failing hearts (28), the JPh44 fragment is therefore “stress-adaptive”.

Materials and Methods

Patients

All patients were recruited and studied in the Malignant Hyperthermia Investigation Unit (MHIU) of the Canadian University Health Network, at Toronto General Hospital, in Toronto, Canada, under protocol 12-5474, last reviewed on 11/08/21. All patients consented to all aspects of the study, including publication. The use of tissue and the language of the informed consent were also approved by the Institutional Review Board of Rush University under protocol 16050502-IRB01. Patients were diagnosed with the CHCT and studied over the last 5 years. Criteria for recruitment of subjects included one or more of the following: a previous adverse anesthetic reaction, family history of MH without a diagnostic MH mutation (www.emhg.org), a variant of unknown significance (VUS) in *RYR1* or *CACNA1S*, recurrent exercise- or heat-induced rhabdomyolysis and idiopathic elevation of serum creatine kinase.

The anonymized demographic data of the 44 individuals whose tissues were used for analyses, imaging or development of cultures, is provided in a supplemental table.

Primary cultures

Biopsied segments of human *Gracilis* muscle were shipped to Rush University at 4°C overnight in an optimized solution of composition described in (21). Primary cultures, derived from the biopsies as described by Censier et al. (84), were maintained at 37°C in a humid atmosphere containing 5% CO_2. After 8–15 days, cells derived from the explants were transferred to a culture dish for proliferation in a growth medium. Myoblasts were expanded through up to four passages. For calcium concentration measurements in live cells, myoblasts were reseeded on collagen-coated dishes (MatTek, Ashland, MA, USA). For immunostaining experiments, myoblasts were seeded on 13 mm coverslips in 24 well plates. At 70% confluence, the cells were switched to a differentiation medium (DMEM-F12 with 2.5%horse serum). Studies were carried out 5–10 days thereafter, in myotubes showing a similar degree of maturation.

C2C12 cultures

The mouse myogenic C2C12 cell line was obtained from ATCC (http://www.atcc.org/) and cells were used until passage number 20. Myoblasts were cultured in Dulbecco's modified Eagle's medium (DMEM) supplemented with 15% fetal bovine serum and 1% penicillin-streptomycin in a humidified incubator kept at 37 °C and 5% CO_2. C2C12 myotubes were obtained by culturing 70% confluent myoblasts in differentiation medium (DMEM, 2% horse serum, 1% penicillin-streptomycin) for at least 4 days.

Transfections and vectors

Transient transfections of C2C12 myoblasts were performed upon reaching 70% confluence using the K2 Transfection System (Biontex Laboratories GmbH, Munich, Germany) as described by the manufacturer. C2C12 myotubes and biopsy-derived human primary myotubes were transfected with plasmids using lipofectamine 3000 (Thermofisher, Waltham, MA, USA) following the supplier's instructions.

Plasmids used in this study such as empty vector for GFP-JPh1, dual tagged JPh1 plasmid (GFP-JPh1-FLAG), and GFP tagged plasmid with JPh44 translating region (GFP-Δ(1-240) JPh1) were created by OriGene Technologies (Rockville, MD, USA). p3XFlag-CAPN1 was a gift from Yi Zhang (Addgene plasmid # 60941; http://n2t.net/addgene:60941 ; RRID:Addgene_60941).

Use of murine muscle

This study was performed in strict accordance with the recommendations in the Guide for the Care and Use of Laboratory Animals of the National Institutes of Health. All of the animals were handled according to approved institutional animal care and use committee (IACUC) of Rush University under protocols (#17-035, 18-065 and 21-068.) 6–10 wk-old mice, *Mus musculus*, of the Black Swiss strain, sourced at Charles River Laboratories (Boston, MA, USA), were used to define the localization of JPh1 and JPh44 in living cells. Hind paws were transfected with plasmid vector for GFP-JPh1, dual tagged JPh1 plasmid (GFP-JPh1-FLAG), and GFP tagged plasmid with JPh44 translating region (GFP-Δ(1-240) JPh1) as described in (85). Transfection required electroporation via intramuscular electrodes, which was performed under anesthesia. Animals were euthanized and muscles collected and processed for imaging as in (86). Every effort was made to minimize animal suffering and discomfort.

Diagnosis of Malignant Hyperthermia Susceptibility

Susceptibility to MH was diagnosed at the MHIU following the North American CHCT protocol (Larach, 1989). Increases in baseline force in response to caffeine and halothane (F_C and F_H) were measured on freshly excised biopsies of *Gracilis* muscle with initial twitch responses that met viability criteria. Three muscle bundles were exposed successively to 0.5-, 1-, 2-, 4-, 8- and 32-mM caffeine; three separate bundles were exposed to 3% halothane. The threshold response for a positive diagnosis was either $F_H \geq 0.7$ g or F_C (in 2-mM caffeine) ≥0.3 g. Patients were diagnosed as 'MH-negative' (MHN) if the increase in force was below threshold for both agonists, and 'MH-susceptible' (MHS) if at least one exposure exceeded the threshold. While prior work distinguishes the muscles that respond excessively to halothane but not to caffeine (named "HH") from those that respond to both (the "HS"), in the present work the distinction is not made, and both groups together are classified as MHS.

Cytosolic calcium concentration

Cytosolic Ca^{2+} concentration, $[Ca^{2+}]$cyto, was monitored in myotubes by shifted excitation and emission ratioing (87) of indo-1 fluorescence as described in (88). Imaging was by confocal microscopy (scanner TCS SP2; Leica Microsystems; Buffalo Grove, IL, USA), using a 63X 1.2 numerical-aperture water-immersion objective. $[Ca^{2+}]_{cyto}$ was derived from fluorescence signals (89). Indo-1 was procured from Invitrogen, Waltham, MA, USA.

Analysis of calpain activity

For in vitro JPh1 cleavage experiments, the whole biopsied muscles from human subjects were homogenized in RIPA lysis buffer (Santa Cruz Biotechnology, Dallas, TX, USA) with protease and phosphatase inhibitors, and the supernatant of centrifugation at 13,000 g for 15 min was used for further process. The cleavage of JPh1 was induced by incubating 100 micrograms of protein supernatants with 0.3–1.0 µg of purified human erythrocyte calpain1 of activity 1 unit/µg (MilliporeSigma, Burlington, MA, USA) at 30^0C for 15 minutes. Supernatants are treated with or without DMSO dissolved 10 µg calpain inhibitor (MDL28170, Cayman Chemical Co., Ann Arbor, MI, USA). SDS sample buffer was added to stop the reaction.

Protein fractionation and Western blotting

Human biopsied muscle segments received from the MHIU were quick-frozen for biochemical studies and storage. For measuring total content of proteins in muscle, the tissue was chopped into small pieces in RIPA lysis buffer (Santa Cruz Biotechnology, Dallas, TX, USA) containing protease and phosphatase inhibitors, and homogenized using a Polytron

disrupter. The homogenate was centrifuged at 13000 g for 10 min and supernatant aliquots were stored in liquid nitrogen. Nuclear and cytosolic protein fractions from muscle biopsies were prepared using NE-PER™ Nuclear and Cytoplasmic Extraction Kit (Catalog. No 78835; ThermoFisher) according to the manufacturer instructions with the help of Dounce homogenizer.

Protein content was quantified by the BCA assay (ThermoFisher). Proteins were separated by SDS–polyacrylamide gel electrophoresis, using 10% mini gels and 26-well pre-cast gels (Criterion TGX, Bio-Rad, Hercules, CA, USA), which enable separation in a broad range of molecular weights, and transferred to a nitrocellulose membrane (Bio-Rad). Membranes were blocked at 4.5% blotting grade (Bio-Rad) in PBS and incubated with the primary antibody overnight at 4°C. Thereafter they were washed in PBS containing 0.1% Tween 20 and incubated in horseradish peroxidase–conjugated anti-mouse or anti-rabbit secondary (Invitrogen, Carlsbad, CA, USA) for 1 hr at room temperature. The blot signals were developed with chemiluminescent substrate (MilliporeSigma) and detected using the Syngene PXi system (Syngene USA Inc, Frederick, MD, USA).

Immunoblot analysis was conducted using the following antibodies (antigen, commercial ID number, concentration, supplier): JPh1 “antibody A”, #PA5-52639, 1:1000, ThermoFisher; JPh1 “antibody B”, #40-5100, 1:1000, ThermoFisher; GSK3β , #9315, 1:1000, Cell Signaling Technology (Danvers, MA, USA); calpain1, #MA1-12454, 1:1000, ThermoFisher; histone H3, #4499, 1:1000, Cell Signaling.

Quantitative analysis of Western blots was done with a custom application (written in the IDL platform, Harris Geospatiale, Paris, France; fully described and demonstrated with video in (22)) that combined information in the blot and the source gel. This method had less variance than the commercial (Syngene) software tools. The content of interest was measured in the blot by the signal mass within a rectangle that enclosed the protein band above a background. A normalization factor, quantifying the sample deposited in the lane, was computed on the gel as the average signal in a large area of the corresponding lane above background. A more advanced version was developed to automatically quantify closely-spaced dual bands (as in Fig. 4E); its use is illustrated in supplemental Fig. 1 to Fig. 4.

Two anti-JPh1 antibodies, A and B, both supplied by ThermoFisher, serendipitously showed different reactivity. When used in Western blots, antibody A (#PA5-52639) reacted almost exclusively with the full-size, ~72 kDa molecule (e.g., Fig.1 A), while antibody B (#40-5100) marked exclusively JPh44 (supplemental Fig. 1 to Fig. 1). This distinctive reactivity was reproduced in staining of adult muscle (e.g., compare panels Ab and Bb in Fig. 2), but not in myotubes, where antibody A stained both junctophilin forms (e.g., Fig. 2 Db) while antibody B retained its specific reactivity for JPh44 (e.g., Fig. 2 Eb).

Immunostaining of human and mice myofibers, and skeletal muscle cell cultures

Immunofluorescence imaging was done on thin myofiber bundles dissected from human muscle biopsies, FDB muscles from mice, primary human myotubes, C2C12-line myotubes and C2C12 myoblasts. Human or mouse muscles were mounted moderately stretched in relaxing solution, on Sylgard-coated dishes. Relaxing solution was replaced by fixative containing 4% PFA for 20 min. Myotubes or myoblasts on coverslips were washed in 1X PBS and fixed with 2% PFA for 20 min. Tissues or cell cultures on coverslips were transferred to a 24-well plate and washed three times for 10 min in PBS, then permeabilized with 0.1% Triton X-100 (Sigma) for 30 min at room temperature and blocked in 5% goat serum (Sigma) with slow agitation for 1 hr. The primary antibody was applied overnight at 4°C with agitation, followed by 3 PBS washes for 10 min. Fluorescent secondary antibody was applied for 2 hr at room temperature. Dehydrated tissues or cell

culture coverslips were mounted with anti-fade medium (Prolong Diamond, ThermoFisher). Immunofluorescence imaging used the following antibodies (antigen, commercial ID number, concentration, supplier): JPh1 "antibody A", #PA5-52639, 1:100, ThermoFisher; JPh1 "antibody B", #40-5100, 1:100, ThermoFisher; calpain1, #MA1-12454, 1:1000, ThermoFisher; Ryr1, #34C, 1:200, ThermoFisher.

High-Resolution imaging of fluorescence

Immunostained myofibers and cell cultures, as well as live tissues expressing fluorescently tagged proteins were imaged confocally using a Falcon SP8 laser scanning system (Leica Microsystems) with a 1.2-numerical aperture, water-immersion, 63x objective. Resolution was enhanced by high sensitivity hybrid GaAsP detectors (HyD, Leica), which allowed low intensity illumination for image averaging with minimum bleaching, optimal confocal pinhole size (below 1 Airy disk), collection of light in extended ranges (e.g., 470-580 nm), and acquisition of *z*-stacks (vertical sets of x-y images) at oversampled *x–y–z* intervals. The stacks usually included 40 x-y images at 120 nm z separation and 60 nm x-y pixel size or, for highest resolution imaging, 20 x-y images at 120 nm z and 36 nm x-y pixel size. Dual images were interleaved by line. Most cells were triply stained and correspondingly monitored at (excitation/emission) (405/ 430-470 nm), (488/500–550 nm) and (555/570–620 nm). The stacks were acquired starting nearest the objective, at or closely outside the lower surface of the myofiber.

Availability of stacks allowed for offline deblurring by a constrained iterative deconvolution algorithm that used all images in the stack (90,91) and the point spread function (PSF) of the system, which was determined using 170-nm beads. PSF FWHM was 350 nm in *x–y* and 480 nm in *z*. After deblurring, the separation effectively resolved in the x-y plane was approximately 0.1 µm (Supplement 11 in (22)). The deblurred set was represented or "rendered" in three dimensions using the "Simulated Fluorescence Process" (92) applied to the full deblurred stack. Determination of the point spread function (PSF) of the imaging system, deblurring, and rendering were done in the HuPro (SVI, Amsterdam, The Netherlands) programming environment.

Location and colocalization analyses

Location analysis defined densities of protein content within nuclei or in extra-nuclear areas (named "cytosol"), by the ratio of integrated fluorescence signal over area in the respective regions. For comparisons among replications the ratio (nuclear/cytosolic) was used, as it was insensitive to inter-preparation variance in expression or staining intensity.

Colocalization (of JPh1, its fragment JPh44, its expressed constructs GFP-JPh1-FLAG, (N)Myc-JPh1 and GFP-Δ(1-240)JPh1, calpain1, its expressed construct (N)FLAG-calpain1 and RyR1) was evaluated by 4 techniques: (1) the Pearson correlation coefficient, calculated as:

$$R = \frac{\sum_i \left(A_i - \bar{A}_i\right)\left(B_i - \bar{B}_i\right)}{\sqrt{\left(A_i - \bar{A}_i\right)^2 \left(B_i - \bar{B}_i\right)^2}} \qquad (1)$$

where A_i and B_i are intensities of two signals in the same pixel i, $\bar{A}_i$ and $\bar{B}_i$ the averages over all pixels, and the summation is extended to all pixels, or a ROI when the entire image is not usable. Subtler, but statistically significant differences in colocalization were detected using the Intensity Correlation Analysis (ICA) introduced by Li et al. (36). This

analysis produces a quantitative measure, the Intensity Correlation Quotient, ICQ, a correlation measure with a definition that reduces the influence of heterogeneous staining of protein expression.

$$ICQ = \frac{\sum_i Sign\left[\left(A_i - \bar{A}_i\right)\left(B_i - \bar{B}_i\right)\right]}{N(pixels)} - 0.5 \qquad (2)$$

The numerator contributes a 1 for every pixel where both signals are above or below average and a -1 for the situation where the differences are opposite. The ratio is normalized to 1 and the subtraction of 0.5 moves the range to [-0.5, 0.5], with the extremes corresponding to perfect exclusion and perfect colocalization. The ICA approach includes a graph, (with examples in panels Fig. 2Cb, d), that plots for every pixel the product $\left(A_i - \bar{A}_i\right)\left(B_i - \bar{B}_i\right)$, or "pixel covariance" of A and B, vs. the intensity of either A or B. The result is strikingly different for cases of colocalization, where the points draw a noisy parabola (e.g., 2Cb) or lack of it (e.g., 2Cd), where points to the left of the abscissa 0 correspond to mutual exclusion of the two signals.

The conventional correlation analyses have no provision for identifying the anisotropic de-localization of particles, which, if systematic, may reflect an actual association, with systematic displacement. This sensitivity to vectorial displacement is achieved here using an approach of Van Steensel et al. (37), which again produces a plot and, in this case, two numerical outputs of interest. The approach (illustrated in Fig. 2 Ca, c) plots the correlation coefficient *R* between image A and image B shifted in one direction (say, *x*, defined as the longitudinal direction in myofibers) by variable amounts *dx*. The "Van Steensel plot" thus plots *R* (*dx*) vs. *dx*. represented by individual symbols in Fig. 2Ca. When the two signals are colocalized, the plot is narrow, and centered at dx = 0. If not, the plot displaces its peak (when the delocalization occurs in a preferred direction) and its width increases. Two numerical quantifiers can be derived on a Gaussian fitted to the points: the abscissa of the maximum (here the "VS shift") and the FWHM. These quantifiers reveal vectorial aspects of the relationship between the two markers. The VS shift gives a rough measure of distance when the separation of the molecules has some vectorial regularity and sidedness. The FWHM is a measure of dispersion of one marker or both. Combined with the high spatial resolution achieved in our images, it allows to detect effects of interventions that fail to cause significant changes by conventional colocalization measurements.

Colocalization measures and plots were implemented with custom programs written in the IDL platform or with the ImageJ "plugin" JACoP (93).

Digital gene expression sequencing

RNA was isolated from GFP-empty vector-transfected and GFP-Δ(1-240) JPh1-transfected C2C12 myoblasts using the RNeasy plus mini kit (Qiagen, Hilden, Germany), based on manufacturer instructions . Samples were processed by LC Sciences (Houston, TX, USA). Processing included the generation of a library and sequencing of transcripts and their identification in the mouse genome (UCSC mm10). A cDNA library constructed from the pooled RNA from C2C12 cell samples of mouse species was sequenced run with Illumina Novaseq TM 6000 sequence platform. Raw paired-end RNA-seq data were firstly subjected to Cutadapt v1.9 to remove reads with adaptor contamination, low quality bases and undetermined bases. Filtered reads were aligned using HISAT2 to generate alignments tailored for transcript assembler. The mapped reads of each sample were assembled using StringTie with default parameters. Then, all transcriptomes from all samples were merged to reconstruct a comprehensive transcriptome using Gffcompare. After the final

transcriptome was generated, StringTie and Ballgown were used to estimate the expression levels of all transcripts and perform expression abundance for mRNAs, by calculating FPKM (fragment per kilobase of transcript per million mapped reads). Differential expression analysis was performed by DESeq2 software between two groups. The genes with the parameter of false discovery rate (FDR) below 0.05 and absolute fold change ≥ 2 were considered differentially expressed. Differentially expressed genes were then subjected to enrichment analysis of GO functions and KEGG pathways.

qRT-PCR assays

RNA extraction and real-time quantitative PCR (qPCR): For qPCR, total RNA was isolated from C2C12 myoblasts transfected with GFP-empty vector or GFP-Δ(1-240)JPh1 using the RNeasy-plus mini kit (QIAGEN) according to the manufacturer's instructions. cDNA was synthesized using the iScript gDNA clear cDNA synthesis kit (BIORAD) according to the manufacturer's instructions. The cDNA was then analyzed via real-time qPCR using the SYBR Green qPCR Master (BIORAD) with the ViiA™ 7 Real-Time PCR System, equipped with a *FAST* 96-well heated block (Applied Biosystems, Life Technologies). Expression levels of HPRT were used as an internal control to normalize the expression of different genes. Quantification was performed by the $2^{-\Delta\Delta Ct}$ method. The qPCR primers used in this study are provided in the "Resources" table.

Replications and Statistics

With few exceptions, due to limitations in the availability of human samples or their derived cultures, imaging and quantitative analyses were replicated in multiple cells from multiple individuals (biological replicates). In figures and tables, the numbers of individuals (patients, mice) is represented by N and the total numbers of cells by n. When multiple cells derive from multiple individuals, statistical measures are derived by hierarchical (nested) analysis implemented in the R environment (94). Significance of differences of averages or paired differences is established using the two-tailed Student's t test, or, when the distributions of compared measures do not satisfy tests of normality and equal variance, the Mann-Whitney Rank Sum test. Correlation between variables is quantified by the first-order correlation coefficient R; this number is always accompanied by an estimate p of the probability of no correlation, a function of R and the sample size, is calculated as described in (22). In tables, sample medians are always provided after sample averages, to afford a first idea of the distribution.

The human samples for protein quantification include 12 "normal" and 13 "HS" individuals selected at random from available samples that satisfy size and preservation criteria. The numbers were chosen for efficiency (as they complete a 25 lane electrophoresis chamber), for consistency with prior work (22), and after analysis that evinced power consistent with study goals (a power of 0.8 for detecting differences of averages of 30%, with standard deviations of 27% at α = 0.05, is achieved with a sample size of 24, 12 each).

There was no blinding and no exclusion criteria other than adequate size and preservation of the sample — no discoloration or gross damage — evaluated visually upon receipt of the biopsy.

Key resources

Reagent type (species) or resource	Designation	Source or reference	Identifiers	Additional information
antibody	Anti-JPh1“antibodyA” (Rabbit Polyclonal)	Thermo Fisher scientific	Catalog # PA5-52639	Dilution: IF: (1:200), WB: (1:1000)
antibody	Anti- JPh1“antibody” (Rabbit Polyclonal)	Thermo Fisher scientific	Catalog #40-5100,	Dilution: IF: (1:200), WB: (1:1000)
antibody	Anti- GSK3β (Rabbit Monoclonal)	Cell Signaling Technology	Catalog #9315	Dilution: WB: 1:1000
antibody	Anti- calpain1 (Mouse Monoclonal)	Thermo Fisher Scientific	Catalog # MA1-12434	Dilution: IF: (1:100), WB: (1:1000)
antibody	Anti-histone H3 (Rabbit Monoclonal)	Cell Signalling Technology	Catalog #4499	Dilution: WB: 1:2000
antibody	Anti-Ryr1 (Mouse polyclonal)	Invitrogen	Catalog #MA3-925	Dilution: IF: 1:200
antibody	Anti-FLAG (Mouse Monoclonal)	Thermo Fisher Scientific	Catalog #MA1-91878	Dilution: IF: 1:200
antibody	Anti-Myc tag antibody (Mouse Monoclonal)	Thermo Fisher Scientific	Catalog # 13-2500	Dilution: IF: 1:200
Recombinant DNA reagent	GFP-JPh1-FLAG Plasmid	OriGene Technologies		
Recombinant DNA reagent	Myc-JPh1 Plasmid	Dr. Sorrentino’s laboratory		
Recombinant DNA reagent	GFP-Δ(1-240) JPh1 Plasmid	OriGene		
Recombinant DNA reagent	p3XFlag-CAPN1 plasmid	Addgene	Catalog # #60941	
biological sample (*Homo-sapiens*)	*Gracilis* muscle	Toronto General Hospital		
Sequence based reagent	Primers (5’ to 3’)	IDT	Hprt	

	Fw: ATGGACTGATTATGGACAGGACTG Rev: TCCAGCAGGTCAGCAAAGAAC			
Sequence based reagent	Primers (5' to 3') Fw: GAGCCACTGATTACACGTCCAG Rev: CCAACTGATCCACACCACTGTC	IDT	Gsk3b	
Sequence based reagent	Primers (5' to 3') Fw: CCCATGATCAAACTGCAGAAAC Rev: GCACTCAACTCACTCCTTAGAA	IDT	Traf3	
Sequence based reagent	Primers (5' to 3') Fw: GTCTTCAGGCAGAGGAAGAAC Rev: GATTTGCCCTGGTACCTCAA	IDT	Repin1	
Sequence based reagent	Primers (5' to 3') Fw: CTGACAACCTCATTCCTGTCTATT Rev: CTTGCAGCTGTTCCATCTC	IDT	Ngfr	
Cell lines	C2C12 Myoblasts	ATCC	CRL-1722	
Protein	Calpain 1 protein from human Erythrocytes	Millipore Sigma	Catalog # 208713	
Drug	Calpain Inhibitor MDL-28170	Cayman	Item No #14283	

Availability of raw data

All quantitative raw data, as well as statistical processing are contained in "JNB" (Sigmaplot) and "XLSX" (Excel) annotated worksheets, publicly available in Harvard Dataverse as "Study on junctophilin 1 and calcium stress" at https://dataverse.harvard.edu/dataverse/Junctophilin1_and_calcium included in dataset "Raw and processed numerical data". All raw image sets are in the same Dataverse, included in dataset "Raw image sets for Junctophilin 1 and calcium stress". For ease of access, a "data trace" line is added to every figure and table legend, identifying the corresponding raw data in the Dataverse. Individual files in the Dataverse contain annotations for traceback to figures and tables in the article.

Raw Western blots and Ponceau-stained originating gels are available as Source Data, as follows:

Figure 1-source data 1. JPh1 raw blot shown in Fig 1A

Figure 1-source data 2. gel for JPh1 blot in figure 1A.

Figure 1-source data 3. JPh44 raw blot shown in Fig 1B

Figure 1-source data 4. gel for JPh44 blot of figure 1B

Figure 1-source data 5 Raw blot in Fig 1F

Figure 1-source data 6. gel for blot of figure 1F

Figure 1-figure supplement 1-source data 1: raw blot of JPh1 (abA)

Figure 1-figure supplement 1-source data 2: Originating gel (right half) for raw blot of JPh1

Figure 1-figure supplement 2-source data 1: Different amounts of human muscle total extract, blot stained with Junctophilin abA as presented in Fig. 1- figure supplement 2.

Figure 1-figure supplement 2-source data 2: Different amounts of human muscle total extract, blot with Junctophilin abB as presented in Fig. 1-figure supplement 2.

Figure 1-figure supplement 2-source data 3: Originating gel for blots in Fig. 1-supplement 2. Junctophilin abA blot is obtained from the left half and abB blot is obtained from the right half of the membrane shown.

Figure 3-source data 1 JPh1 raw blot in figure 3D

Figure 3-source data 2. Originating gel for blot in figure 3D

Figure 3-source data 3. Raw blot in figure 3E (boxed region). The bands of upper molecular weight (particularly at 70 kDa) result from earlier incubation of same membrane with JPh1 abA and its incomplete stripping. Last 3 lanes in the blot are unrelated to the experiment.

Figure 3-source data 4. Gel for figure 3E

Figure 3-source data 5. Raw blot for figure 3G

Figure 3-source data 6. Originating gel for blot in figure 3G

Figure 4- source data 1. Raw blot for figure 4D (boxed region). Lower part of the blot, with calpain fragments of small molecular weight is shown in Figure 4- figure supplement 2.

Figure 4- source data 2. Originating gel for blot in figure 4D

Figure 4-figure supplement 2 source data1 : raw blot (boxed area in pdf document).

Figure 4-figure supplement 2 source data2. Originating gel.

Figure 5-source data 1: JPh raw blot incubated with JPh abA shown in figure 5A

Figure 5-source data 2: originating gel for blot shown in figure 5A

Figure 5-source data 3: JPh1 raw blot in figure 5C

Figure 5-source data 4: JPh44 raw blot in figure 5C

Figure 5-source data 5: originating gel for blots in 5C

Figure 5-source data 6: JPh1 blot in figure 5E

Figure 5-source data 7: JPh44 blot in figure 5E

Figure 5-source data 8: originating gel for 5E

Figure 8-source data 1: GSK3b raw blot for figure 8E.

Figure 8-source data 2: GFP-Δ(1-240) JPh1 blot for figure 8E.

Figure 8-source data 3: Originating gel for blots in figure 84. GSK3B blot is derived from the left part and JPh from right part of the membrane.

Availability of Materials and other resources

All newly created materials described in this manuscript, including dual-tagged full-length Junctophilin plasmids and Junctophilin mutant will be available from the corresponding author upon reasonable request. Code for custom program created for the analysis of close doublet bands in Western blots, is attached as Blot_n_rot_double.txt, written in IDL language (Harris Geospatiale, Paris, France).

Supplement

Supplemental materials include:

a PDF document with untrimmed versions of all Western blots and their originating, Ponceau-stained gels, which were used for normalization of the WB bands,

Supplemental figures (3 to Fig. 1, 1 to Fig. 2, 1 to Fig. 3, 2 to Fig. 4, 1 each to figures 5, 6 and 8),

Supplemental videos (6 to Fig. 2 and 3 to Fig. 3)

Table that provides anonymized demographic data of individuals whose tissue was used in this study.

Additional document

Raw Western blots and original gels. A Word document providing all original images of gels and blots, cross-referenced to figures and tables in the manuscript.

1

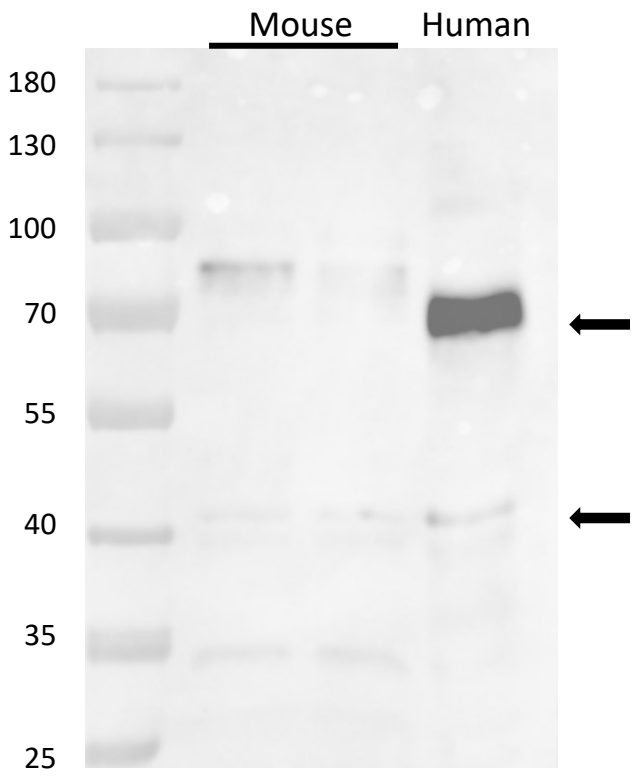

Supplemental Fig. 1 to Fig. 1. Staining of muscle extracts from mice and a human subject, by antibody A, raised against a human JPh1 immunogen (residues 387-512). The antibody tags two proteins at ~72 and ~44 kDa in the human sample, and at ~80 and 44 kDa in the mouse. Data trace:

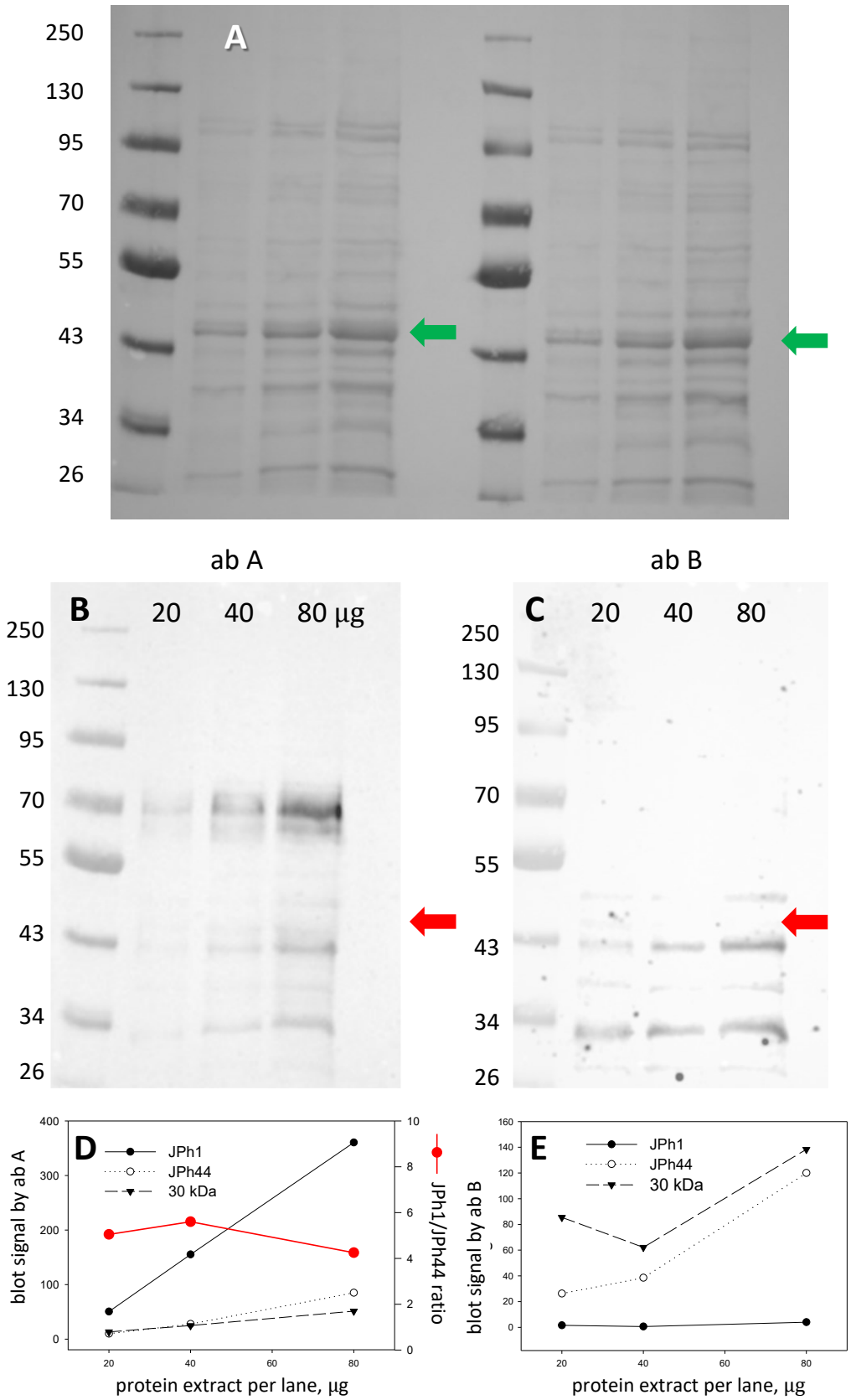

Supplement Fig. 2 to Fig. 1. Specificity of junctophilin antibodies. A, Ponceau-stained gel. Human biopsied muscle was lysed in RIPA buffer. Protein extract was exposed for 5 min at room T to 0.3U calpain/30µg of total protein. The reaction was stopped with loading buffer. 20, 40 and 80 µg of boiled extract, at 2µg/µl, was loaded into PAGE wells as shown B, C, Blots, from left and right halves of gel A, stained with junctophilin antibodies A and B. D, E, Filled circle, signal in main band at ~70 kDa ("JPh1"); open circle, band at ~ 43 kDa ("JPh44"; triangle, at ~30 kDa. Red circle in D, ratio of JPh1 to JPh44 signals, indicating rough proportionality of both ab A signals with well load. By contrast, ab B (panel E) does not react with JPh1. Due to its lack of proportionality with load, the signal at 30 kDa is difficult to assign. Arrows in A mark location of actin, recognizable by its abundance. Red.arrows in B and C are transferred from panel A, to show that the blot signals at ~43 kDa mark a different protein. *Data trace*: images 103022a; subject ID #175 (MHS). Graphs in patient175byA_B_load.JNB.

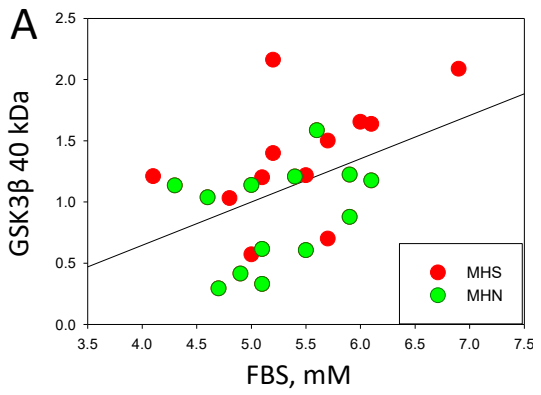

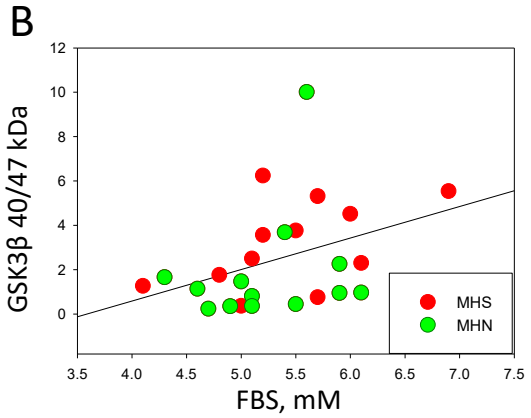

Supp. Fig. 3 to Fig. 1. Plots of Fasting Blood Glucose (FBS) measured in the 25 patients with analysis of GSK3β analysis reported in Fig. 1, vs. the normalized content of truncated (activated) GSK3β (panel A), or the truncated/full-size ratio of contents (panel B). The variables are positively correlated; R = 0.45 for panel A and 0.38 for panel B. The probabilities p of no correlation are 0.02 and 0.06, respectively.

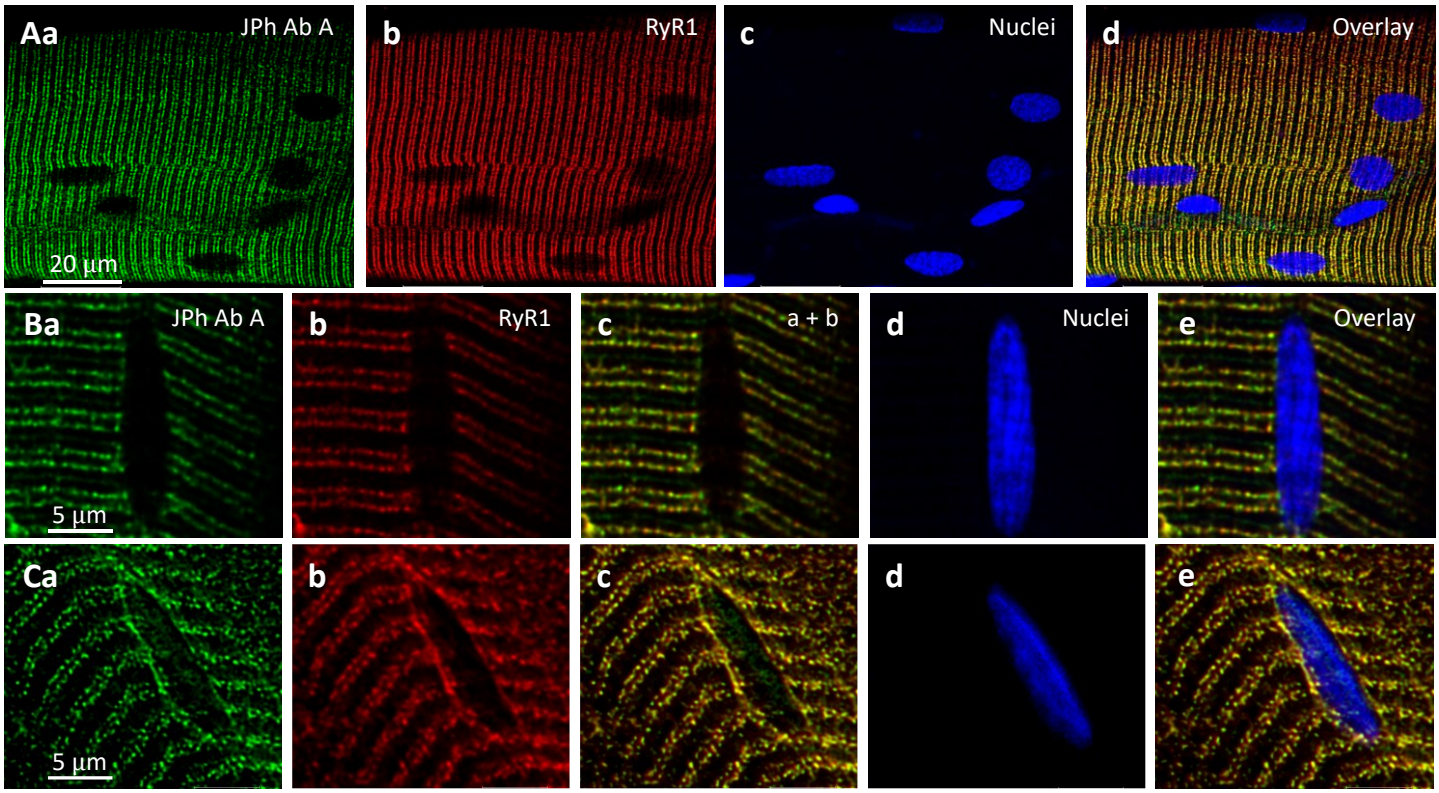

Supplemental Fig. 1 to Fig. 2. IF images from the human fiber bundle illustrated in Fig. 2, stained with the anti-JPh1 ab A, and RyR1 and nuclear markers. Row A shows strong colocalization of ab A and RyR1 signals, and weak or no staining at nuclei. B and C show detail in two regions of the same bundle: in B from a region with conserved structure and triad alignment, and no intra-nuclear ab A staining at this gain. In C, an area of disrupted structure, near visible damage, shows misaligned protein markers and ab A intra-nuclear staining. Based on the ab A signal, the intra-nuclear protein could be JPh1 or its 44 kDa fragment. The strong ab B signal inside nuclei (Fig. 2) and its specificityfor JPh44 (Supplement figs. 1 and 2 to Fig. 1) identify the intranuclear signal in panel Ca as the JPh44 fragment. *Data trace*: Patient ID 167 (HH; same as in Fig. 2), images in 102422La, series 003 (A), 005(B) and 002 (C). All images from z stacks corrected for optical dispersion.

Supplemental videos to Fig. 2.

Videos: #1, ab B, 030120Lb_001, patient #172, MHN; #2, ab B, 121619La_011, patient # 166, HH.

Videos: #3, ab A, 030120La_010, patient #172, MHN; #4, ab A, 072420Lb_011, patient #168, HH.

Videos: #5, ab B, 021220La_008, patient #173, HH; #6, ab A, 102019La_004, patient #166, HH.

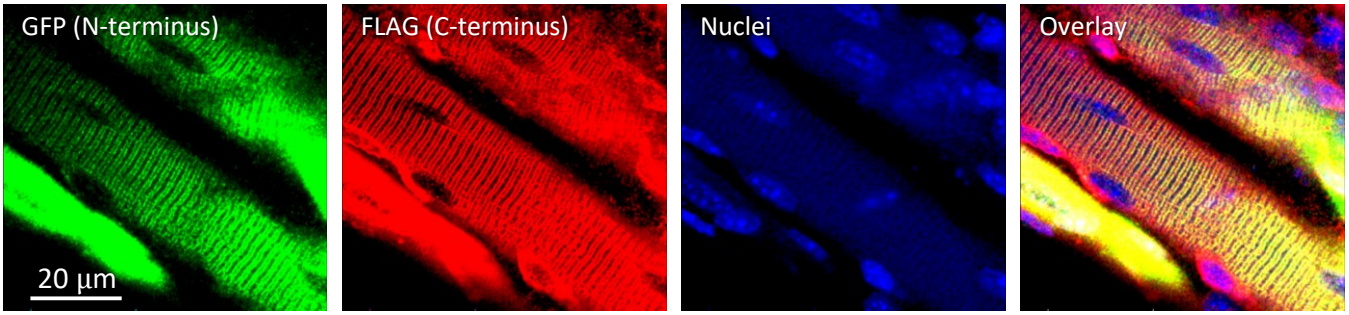

Supplemental Fig.1 to Fig.3. Muscle bundle from adult, presumably normal mouse expressing GFP-JPh1-FLAG. Illustrates location of JPh and its fragments inside nuclei, null for N terminus and variable but scarce for C terminus. Data trace: 100520La_004. Included in revision as Supplemental Fig. 1 to Fig. 3.

Supplemental videos to Fig. 3.

Supp 1 Fig 3 091620La_animatedSeries005.avi, (the full z-stack for panels A in Fig. 3).

Supp 2 Fig 3 091020La_animatedSeries004forFig3.avi, (z-stack for Fig. 3 B).

Supp 3 Fig 3 100520La_animatedSeries002forFig3.avi, (z-stack for Fig. 3 C).

Temp storage: D:\Dropbox\JPh\Revision\review round 1 files\comment 17

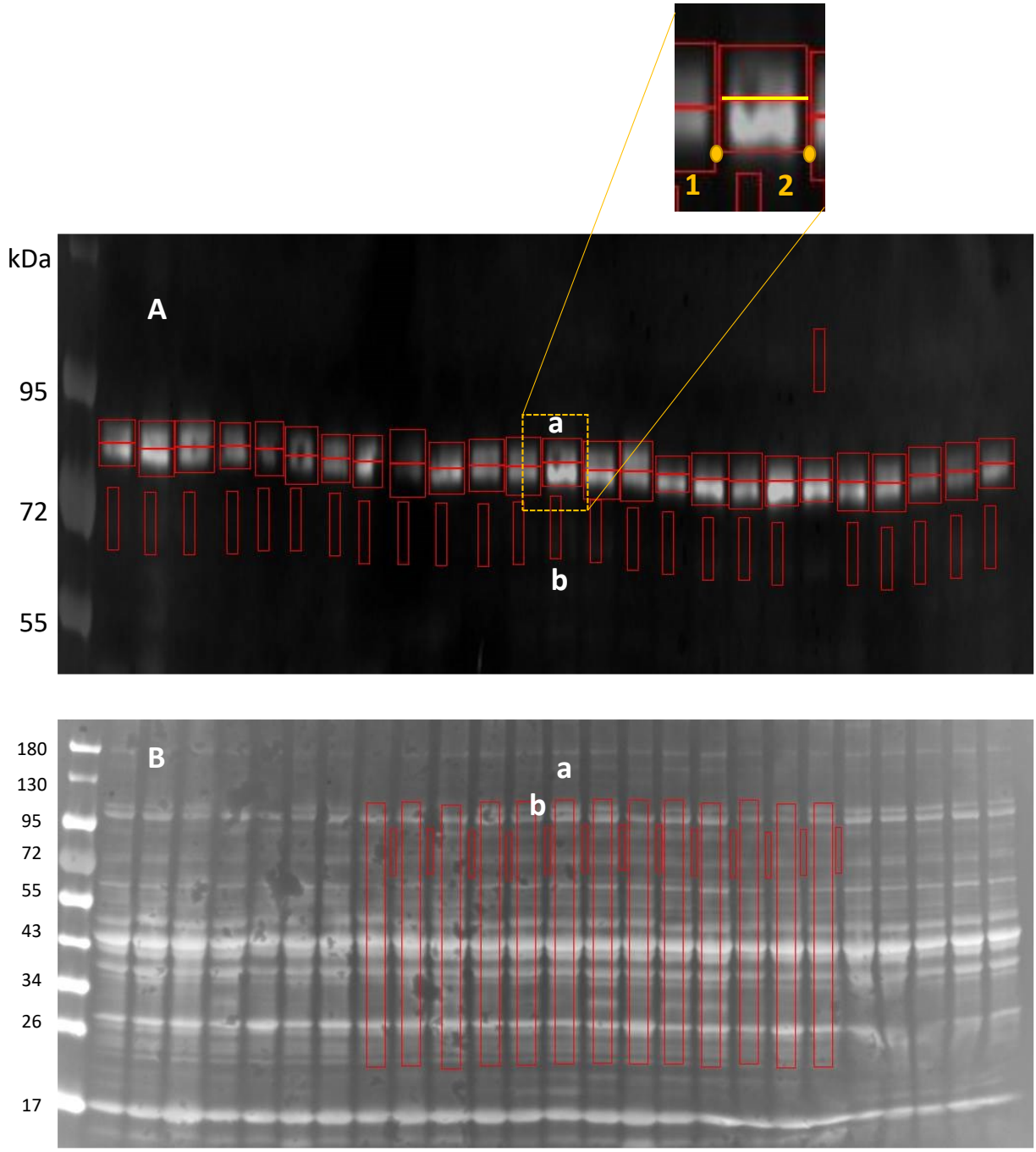

Supp. Fig. 1 to Fig. 4. A streamlined method to quantify double bands in Western blots. The method introduced by Tammineni et al. in (22) was modified for objective analysis of closely placed double bands. A, Western blot, stained for calpain1 (reproduced from Fig. 4E, at 4x magnification in the vertical direction, converted to "positive", i.e., with pixel values corresponding to reporter intensity signal), shows closely placed bands at approx. 80 and 76 kDa. B, the originating gel, at the original magnification. On WB (panel A), working on one column at a time, the user selects a background region "b" and starts the definition of two active region of interest (ROIs) "a" by marking points 1 and 2 (inset), which define the width of the ROIs. The program then locates automatically a border between the two close bands (yellow segment), at the minimum of the bands signal, averaged in the horizontal direction. For columns where the minimum used to define the border in A is ill-defined, the user defines the lower ROI by clicking two diagonal corners, lower left and upper right; the border between the two bands is then defined by the upper corner. Two symmetrical ROIs (red rectangles) are thus defined, where the signals of the two bands are integrated. For normalization to total quantity of protein, the signals are then normalized by the total signal in the corresponding column of the Ponceau-stained gel, calculated as the difference between the signal integrated over active area "a" (in B), after subtraction of background "b". All ROIs "a" in B have the same area. Program code, written in the IDL environment (Geospatiale, Paris, France), is attached as text file "Blot_n_rot_double.txt".

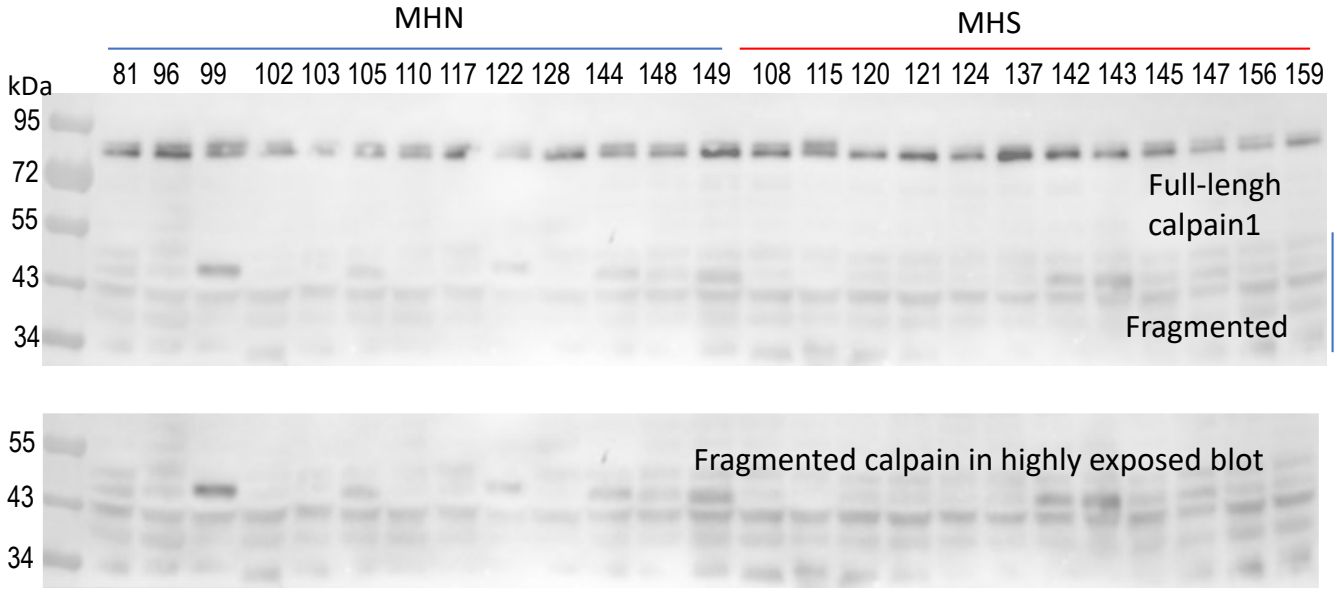

Supp. Fig. 2 to Fig.4. Western blot of calpain1 in whole-tissue protein of human subjects. Same as in Fig. 4 E, extending range to show multiple low-weight fragments. The region of fragments is shown in the bottom panel, developed at higher exposure.

1
2

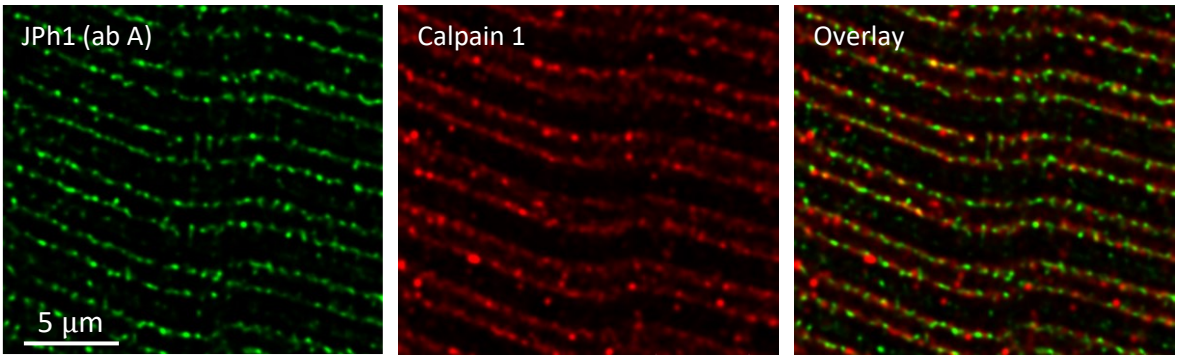

Supplemental Fig. 1 to Fig. 5. Distribution of calpain1 in myofibers from a MHN subject. Muscle bundle co-stained with JPh1 ab A and calpain 1 antibody. Images from z-stacks after correction for optical dispersion. The location at triads and partial colocalization of both markers does not differ visibly from that in Fig. 6, in muscle from a MHS patient. Data trace: 113021La_Series004. Subject ID #220.

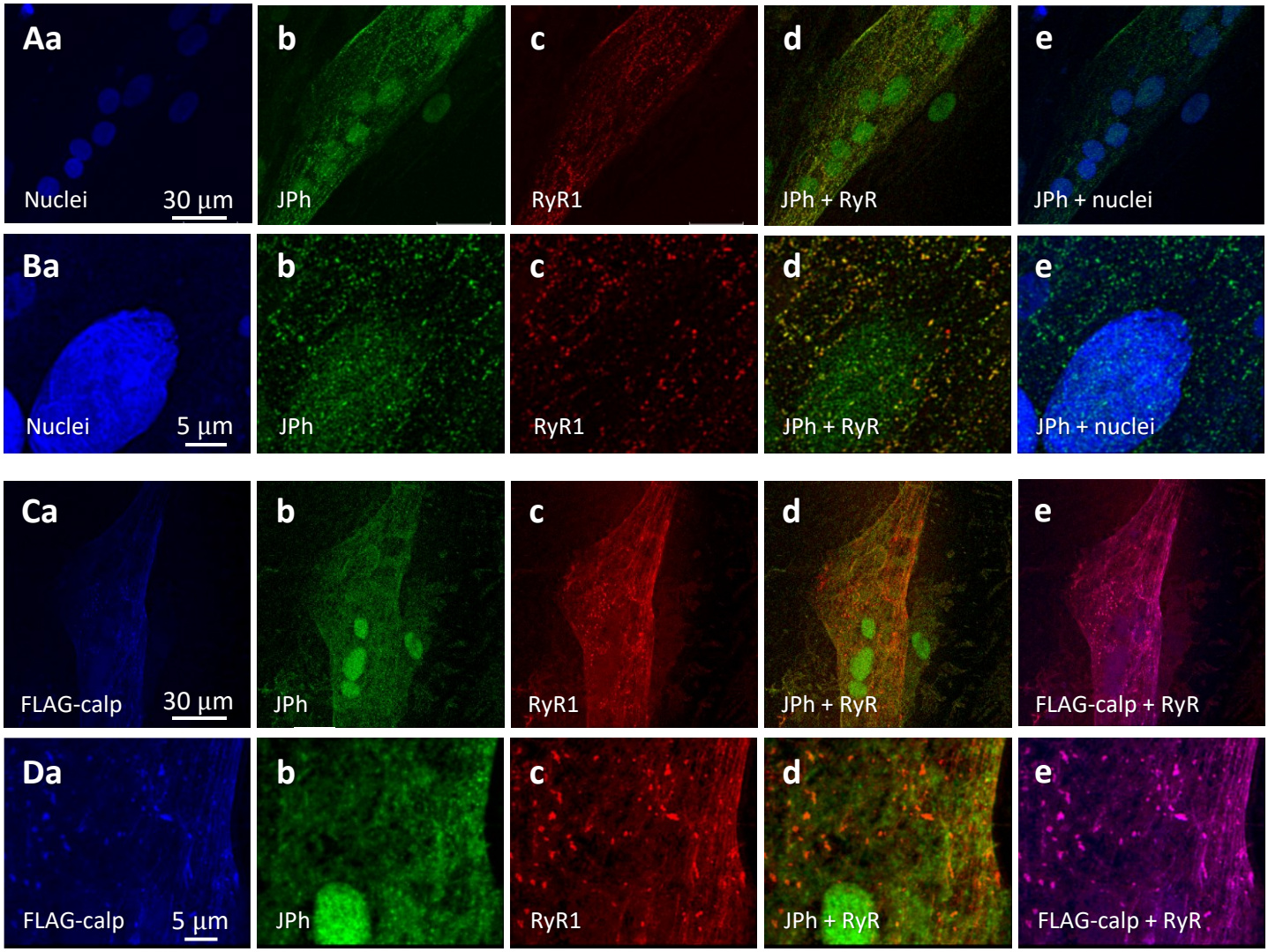

Supplemental Fig. 1 to Fig. 6. Calpain drives nuclear localization of JPh. A, B) Primary myotubes derived from subject # 180 (MHN) were stained with nuclear and RyR1 markers, and JPh1 ab A. JPh1 distributed both in cytosol and nuclei (Ab, e, Bb, e). JPh puncta in cytosol likely corresponds to JPh1, as they colocalized with RyR1. C, D) Myotubes of the same individual, transfected with FLAG-calpain 1. Note loss of the JPh punctated pattern in cytosol and intense JPh ab A signals, of diffuse pattern, inside nuclei. FLAG-calpain is colocalized with RyR in puncta or clusters that likely correspond to developing junctions (Dd, e). As observed in Fig. 6, expression of calpain seems to improve expression and clustering of RyR1. Data trace: A) 073020Lb series 011; B) 073020Lb series 012; C) 073020La series 002; D) 073020La series 003. All images taken from z-stacks corrected for optical dispersion.

1

2

3

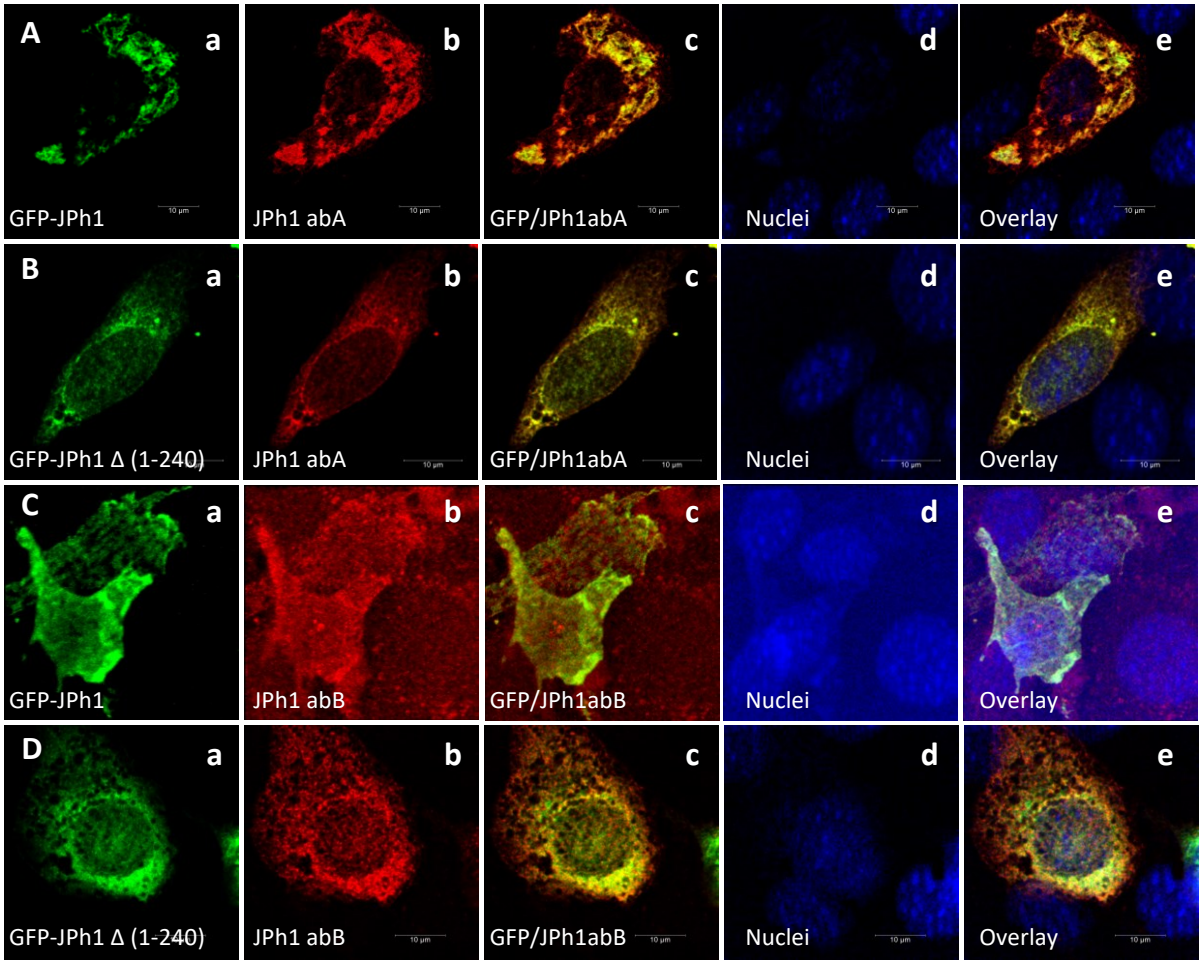

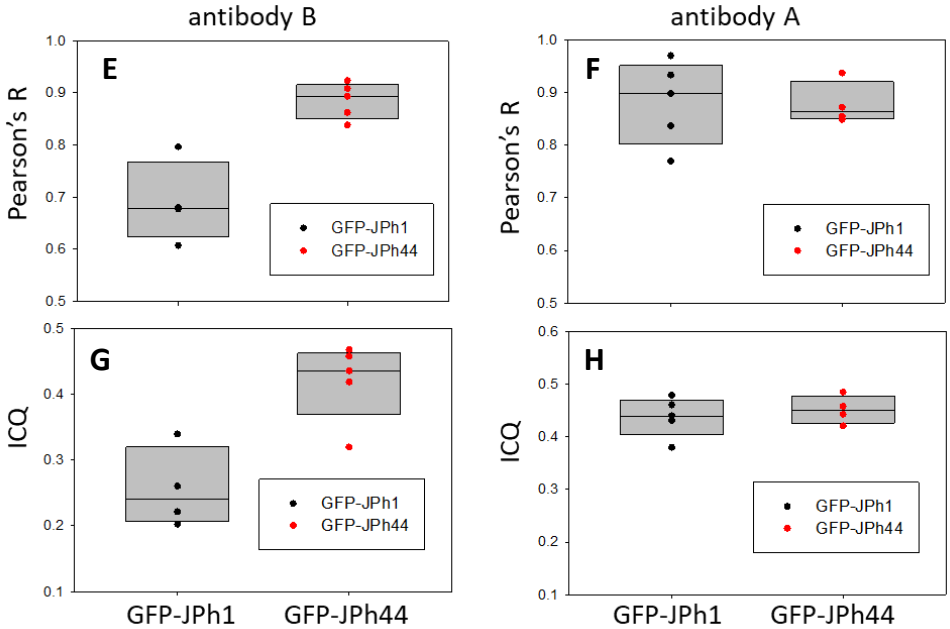

Supplemental Fig. 1 to Fig. 8. Expression of tagged JPh1 and a JPh44 stand-in. A-D, immunofluorescence images of fields of C2C12 cultures expressing either GFP-JPh1 (full-size, rows A, C) or GFP-JPh1 Δ (1-240) (B, D) and stained with ab A (rows A, B) or ab B (C, D). Images show respectively GFP fluorescence, the signal with abs A or B, the overlay of GFP and ab signal, nuclear staining and the triple overlay. Images are single slices from "z-stacks" of 45 x-y images at 60 nm interval, after correction for optical dispersion. Note the lesser colocalization of ab B with GFP in GFP-JPh1-transfected cells (Cc and e). E-H. Colocalization analysis of IF images in A-D. Two measures of colocalization, the correlation coefficient R and the Intensity Correlation Quotient were calculated (Methods). The plots compare their distributions between cultures expressing the two fusion proteins (n = 4 or 5 fields). For brevity, the GFP- JPh1 Δ (1-240) data is labeled "GFP-JPh44". Ab B (E, G) colocalized with GFP-JPh1 much more than with GFP-JPh44 (p = 0.001 for R, 0.005 for ICQ). Ab A (F, H) did not show preference for either construct (p = 0.941 for R and 0.564 for ICQ. 2-tailed t-tests in all cases). Note also that the colocalization values of ab B with the JPh44 construct are similar to those of ab A with either construct. *Data trace*: A, 100522Lc_Series005_Lng_adaptSnap1. B, 100722La_Series004_Lng_adaptSnap1. C, 100522Lb_ series001_Lng_adapt#22. D, 100522La_Series004_Lng_adaptSnap6. Graphs in *JPh/C2C12 JPh1 and 44 by abs B and A.*

1 Supplemental Table

Patient ID	Age/Gender	Ethnicity	CHCT status
81	33/F	First nation/indigenous	HN
96	41/M	Caucasian	HN
98	39/M	Caucasian	HN
99	36/M	Caucasian	HN
102	43/M	Caucasian	HN
103	35/ F	Caucasian	HN
105	29/M	Caucasian	HN
108	20/M	Caucasian	HH
110	21/F	Caucasian	HN
115	36/M	Caucasian	HH
117	39/F	Caucasian	HN
118	31/M	East Asian	HN
120	39/M	Caucasian	HH
121	32/M	Caucasian	HH
122	38/M	Caucasian	HN
124	30/M	Caucasian	HH
128	43/F	Caucasian	HN
137	39/F	Hispanic	HH
140	62/F	Ashkenazie	HN
142	39/F	Caucasian	HH
143	38/F	Caucasian	HH
144	48/M	Caucasian	HN
145	24/M	Indian	HH
147	50/M	Caucasian	HH
148	47/M	Caucasian	HN
149	55/M	Indigenous	HN
152	34/M	Caucasian	HN
154	33/M	Ashkenazie	HH
155	34/F	Caucasian	HN
156	M	Hispanic	HS
158	20/M	Caucasian	HN
159	18/M	Caucasian	HH
160	18/M	Caucasian	HS
161	39/M	Caucasian	HN
162	25/F	Caucasian	HH
163	38/M	Caucasian	HN
164	31/F	First nation/indigenous	HN
165	35/M	Caucasian	HN
166	21/M	Caucasian	HS
167	39/M	Caucasian	HH
168	21/M	Caucasian	HH
169	48/M	Presumed Caucasian (Adopted)	HH
170	24/F	Caucasian	HN
172	34/F	Caucasian	HN

Template frame do not erase

173	38/M	Caucasian	HH
175	29/F	Caucasian	HH
176	30/F	Caucasian	HN
179	22/F	Chinese	HS
180	21/F	Caucasian	HN
184	60/F	Caucasian	HN
187	35/M	Caucasian	HN
189	59/M	Caucasian	HS
190	54/M	Caucasian	HH
194	24/F	Caucasian	HN
223	30/F	Caucasian	HN
224	48/M	Caucasian	HS

Demographic information for all patients whose samples were analyzed for this study. Col 1: ID #; Col 2: Test date; Col 3: Age/sex; Col 4: ethnicity or race; Col 5: CHCT diagnostic category, nomenclature introduced by (22): HN, normal; HH, hyperreactive to halothane only; HS, hyperreactive to both halothane and caffeine. * First nation/indigenous.

References

1. Stern MD, Pizarro G, Ríos E. Local control model of excitation-contraction coupling in skeletal muscle. J Gen Physiol. 1997 Oct;110(4):415–40.

2. Franzini-Armstrong C, Protasi F, Ramesh V. Shape, size, and distribution of Ca(2+) release units and couplons in skeletal and cardiac muscles. Biophys J. 1999 Sep;77(3):1528–39.

3. Perni S, Lavorato M, Beam KG. De novo reconstitution reveals the proteins required for skeletal muscle voltage-induced Ca2+ release. Proc Natl Acad Sci U S A. 2017 26;114(52):13822–7.

4. Wu F, Quiñonez M, DiFranco M, Cannon S. Stac3 enhances expression of human CaV1.1 in Xenopus oocytes and reveals gating pore currents in HypoPP mutant channels. J Gen Physiol. 2018;

5. Takeshima H, Komazaki S, Nishi M, Iino M, Kangawa K. Junctophilins: a novel family of junctional membrane complex proteins. Mol Cell. 2000 Jul;6(1):11–22.

6. Komazaki S, Ito K, Takeshima H, Nakamura H. Deficiency of triad formation in developing skeletal muscle cells lacking junctophilin type 1. FEBS Lett. 2002 Jul 31;524(1–3):225–9.

7. Rossi D, Scarcella AM, Liguori E, Lorenzini S, Pierantozzi E, Kutchukian C, et al. Molecular determinants of homo- and heteromeric interactions of Junctophilin-1 at triads in adult skeletal muscle fibers. Proc Natl Acad Sci U S A. 2019 30;116(31):15716–24.

8. Litman RS, Griggs SM, Dowling JJ, Riazi S. Malignant Hyperthermia Susceptibility and Related Diseases. Anesthesiology. 2018;128(1):159–67.

9. Ríos E, Figueroa L, Manno C, Kraeva N, Riazi S. The couplonopathies: A comparative approach to a class of diseases of skeletal and cardiac muscle. J Gen Physiol. 2015 Jun;145(6):459–74.

10. Dirksen RT, Avila G. Distinct effects on Ca2+ handling caused by malignant hyperthermia and central core disease mutations in RyR1. Biophys J. 2004 Nov;87(5):3193–204.

11. Lopez JR, Alamo LA, Jones DE, Papp L, Allen PD, Gergely J, et al. [Ca2+]i in muscles of malignant hyperthermia susceptible pigs determined in vivo with Ca2+ selective microelectrodes. Muscle Nerve. 1986 Jan;9(1):85–6.

12. Lopez JR, Gerardi A, Lopez MJ, Allen PD. Effects of dantrolene on myoplasmic free [Ca2+] measured in vivo in patients susceptible to malignant hyperthermia. Anesthesiology. 1992 May;76(5):711–9.

13. Eltit JM, Hidalgo J, Liberona JL, Jaimovich E. Slow calcium signals after tetanic electrical stimulation in skeletal myotubes. Biophys J. 2004 May;86(5):3042–51.

14. Eltit JM, Ding X, Pessah IN, Allen PD, Lopez JR. Nonspecific sarcolemmal cation channels are critical for the pathogenesis of malignant hyperthermia. FASEB J Off Publ Fed Am Soc Exp Biol. 2013 Mar;27(3):991–1000.

15. Manno C, Figueroa L, Royer L, Pouvreau S, Lee CS, Volpe P, et al. Altered Ca2+ concentration, permeability and buffering in the myofiber Ca2+ store of a mouse model of malignant hyperthermia. J Physiol. 2013 Jul 29;

16. Ríos E. The cell boundary theorem: a simple law of the control of cytosolic calcium concentration. J Physiol Sci JPS. 2010 Jan;60(1):81–4.

17. Edwards JN, Friedrich O, Cully TR, von Wegner F, Murphy RM, Launikonis BS. Upregulation of store-operated Ca2+ entry in dystrophic mdx mouse muscle. Am J Physiol Cell Physiol. 2010 Jul;299(1):C42-50.

18. Boittin FX, Petermann O, Hirn C, Mittaud P, Dorchies OM, Roulet E, et al. Ca2+-independent phospholipase A2 enhances store-operated Ca2+ entry in dystrophic skeletal muscle fibers. J Cell Sci. 2006 Sep 15;119(Pt 18):3733–42.

19. Bellinger AM, Reiken S, Carlson C, Mongillo M, Liu X, Rothman L, et al. Hypernitrosylated ryanodine receptor calcium release channels are leaky in dystrophic muscle. Nat Med. 2009 Mar;15(3):325–30.

20. Britt BA. Malignant Hyperthermia: A Review. In: Thermoregulation: Pathology, Pharmacology and Therapy. New York: Pergamon Press; 1991. p. 179–292.

21. Figueroa L, Kraeva N, Manno C, Toro S, Ríos E, Riazi S. Abnormal calcium signalling and the caffeine-halothane contracture test. Br J Anaesth. 2019 Jan;122(1):32–41.

22. Tammineni E, Kraeva N, Figueroa N, Manno C, Ibarra C, Klip A, et al. Intracellular calcium leak lowers glucose storage in human muscle, promoting hyperglycemia and diabetes. eLife. 2020 May 4;2020:9:53999.

23. Altamirano F, Riazi S, Ibarra Moreno CA, Kraeva N, Uryash A, Allen PD, et al. Is malignant hyperthermia associated with hyperglycaemia? Br J Anaesth. 2019 Jan;122(1):e3–5.

24. Murphy RM, Dutka TL, Horvath D, Bell JR, Delbridge LM, Lamb GD. Ca2+-dependent proteolysis of junctophilin-1 and junctophilin-2 in skeletal and cardiac muscle. J Physiol. 2013 Feb 1;591(3):719–29.

25. Takeshima H, Hoshijima M, Song LS. Ca^{2+} microdomains organized by junctophilins. Cell Calcium. 2015 Oct;58(4):349–56.

26. Lehnart SE, Wehrens XHT. The role of junctophilin proteins in cellular function. Physiol Rev. 2022 Jul 1;102(3):1211–61.

27. Perni S. The Builders of the Junction: Roles of Junctophilin1 and Junctophilin2 in the Assembly of the Sarcoplasmic Reticulum–Plasma Membrane Junctions in Striated Muscle. Biomolecules. 2022 Jan;12(1):109.

28. Guo A, Wang Y, Chen B, Wang Y, Yuan J, Zhang L, et al. E-C coupling structural protein junctophilin-2 encodes a stress-adaptive transcription regulator. Science. 2018 21;362(6421).

29. Lahiri SK, Quick AP, Samson-Couterie B, Hulsurkar M, Elzenaar I, van Oort RJ, et al. Nuclear localization of a novel calpain-2 mediated junctophilin-2 C-terminal cleavage peptide promotes cardiomyocyte remodeling. Basic Res Cardiol. 2020 26;115(4):49.

30. Ito K, Komazaki S, Sasamoto K, Yoshida M, Nishi M, Kitamura K, et al. Deficiency of triad junction and contraction in mutant skeletal muscle lacking junctophilin type 1. J Cell Biol. 2001 Sep 3;154(5):1059–67.

31. Wang J, Shi Q, Wang Y, Dawson LW, Ciampa G, Zhao W, et al. Gene Therapy With the N-Terminus of Junctophilin-2 Improves Heart Failure in Mice. Circ Res. 2022 Apr 29;130(9):1306–17.

32. Michelucci A, Paolini C, Boncompagni S, Canato M, Reggiani C, Protasi F. Strenuous exercise triggers a life-threatening response in mice susceptible to malignant hyperthermia. FASEB J Off Publ Fed Am Soc Exp Biol. 2017 Aug;31(8):3649–62.

33. Jin N, Yin X, Yu D, Cao M, Gong CX, Iqbal K, et al. Truncation and activation of GSK-3β by calpain I: a molecular mechanism links to tau hyperphosphorylation in Alzheimer's disease. Sci Rep. 2015 Feb 2;5(1):8187.

34. Goñi-Oliver P, Lucas JJ, Avila J, Hernández F. N-terminal Cleavage of GSK-3 by Calpain: A NEW FORM OF GSK-3 REGULATION *. J Biol Chem. 2007 Aug 3;282(31):22406–13.

35. Ma S, Liu S, Huang Q, Xie B, Lai B, Wang C, et al. Site-specific Phosphorylation Protects Glycogen Synthase Kinase-3β from Calpain-mediated Truncation of Its N and C Termini *. J Biol Chem. 2012 Jun 29;287(27):22521–32.

36. Li Q, Lau A, Morris TJ, Guo L, Fordyce CB, Stanley EF. A syntaxin 1, Galpha(o), and N-type calcium channel complex at a presynaptic nerve terminal: analysis by quantitative immunocolocalization. J Neurosci Off J Soc Neurosci. 2004 Apr 21;24(16):4070–81.

37. van Steensel B, van Binnendijk EP, Hornsby CD, van der Voort HT, Krozowski ZS, de Kloet ER, et al. Partial colocalization of glucocorticoid and mineralocorticoid receptors in discrete compartments in nuclei of rat hippocampus neurons. J Cell Sci. 1996 Apr;109 (Pt 4):787–92.

38. Figueroa L, Kraeva N, Manno C, Riazi S, Rios E. Differential Sensitivity to Halothane Among Subgroups of Malignant Hyperthermia Susceptible Patients: Insights into Dual Pathophysiological Mechanisms. Biophyscial J. 2021;120(3):150a–1a.

39. Yoshimura N, Kikuchi T, Sasaki T, Kitahara A, Hatanaka M, Murachi T. Two distinct Ca2+ proteases (calpain I and calpain II) purified concurrently by the same method from rat kidney. J Biol Chem. 1983 Jul 25;258(14):8883–9.

40. Goll DE, Thompson VF, Li H, Wei W, Cong J. The calpain system. Physiol Rev. 2003 Jul;83(3):731–801.

41. SUZUKI K, TSUJI S, ISHIURA S, KIMURA Y, KUBOTA S, IMAHORI K. Autolysis of Calcium-Activated Neutral Protease of Chicken Skeletal Muscle1. J Biochem (Tokyo). 1981 Oct 1;90(6):1787–93.

42. Moldoveanu T, Hosfield CM, Lim D, Elce JS, Jia Z, Davies PL. A Ca2+ Switch Aligns the Active Site of Calpain. Cell. 2002 Mar 8;108(5):649–60.

43. Liu Z, Cao J, Gao X, Ma Q, Ren J, Xue Y. GPS-CCD: a novel computational program for the prediction of calpain cleavage sites. PloS One. 2011 Apr 20;6(4):e19001.

44. Yang ZF, Panwar P, McFarlane CR, Tuinte WE, Campiglio M, Van Petegem F. Structures of the junctophilin/voltage-gated calcium channel interface reveal hot spot for cardiomyopathy mutations. Proc Natl Acad Sci. 2022 Mar 8;119(10):e2120416119.

45. Murphy RM, Verburg E, Lamb GD. Ca2+ activation of diffusible and bound pools of mu-calpain in rat skeletal muscle. J Physiol. 2006 Oct 15;576(Pt 2):595–612.

46. Murphy RM. Calpains, skeletal muscle function and exercise. In 2009. Available from: http://aups.org.au/Proceedings/40/95-102/#13

47. Goll DE, Thompson VF, Taylor RG, Christiansen JA. Role of the calpain system in muscle growth. Biochimie. 1992 Mar;74(3):225–37.

48. Gómez-Valadés AG, Méndez-Lucas A, Vidal-Alabró A, Blasco FX, Chillon M, Bartrons R, et al. Pck1 gene silencing in the liver improves glycemia control, insulin sensitivity, and dyslipidemia in db/db mice. Diabetes. 2008 Aug;57(8):2199–210.

49. Graham TE, Yang Q, Blüher M, Hammarstedt A, Ciaraldi TP, Henry RR, et al. Retinol-Binding Protein 4 and Insulin Resistance in Lean, Obese, and Diabetic Subjects. N Engl J Med. 2006 Jun 15;354(24):2552–63.

50. Kern M, Kosacka J, Hesselbarth N, Brückner J, Heiker JT, Flehmig G, et al. Liver-restricted Repin1 deficiency improves whole-body insulin sensitivity, alters lipid metabolism, and causes secondary changes in adipose tissue in mice. Diabetes. 2014 Oct;63(10):3295–309.

51. Botteri G, Montori M, Gumà A, Pizarro J, Cedó L, Escolà-Gil JC, et al. VLDL and apolipoprotein CIII induce ER stress and inflammation and attenuate insulin signalling via Toll-like receptor 2 in mouse skeletal muscle cells. Diabetologia. 2017 Nov;60(11):2262–73.

52. Chen Z, Canet MJ, Sheng L, Jiang L, Xiong Y, Yin L, et al. Hepatocyte TRAF3 promotes insulin resistance and type 2 diabetes in mice with obesity. Mol Metab. 2015 Oct 17;4(12):951–60.

53. Lian J, Quiroga AD, Li L, Lehner R. Ces3/TGH deficiency improves dyslipidemia and reduces atherosclerosis in Ldlr(-/-) mice. Circ Res. 2012 Sep 28;111(8):982–90.

54. Baeza-Raja B, Li P, Le Moan N, Sachs BD, Schachtrup C, Davalos D, et al. p75 neurotrophin receptor regulates glucose homeostasis and insulin sensitivity. Proc Natl Acad Sci U S A. 2012 Apr 10;109(15):5838–43.

55. Baeza-Raja B, Akassoglou K. Glucose homeostasis and p75NTR: the sweet side of neurotrophin receptor signaling. Cell Cycle Georget Tex. 2012 Sep 1;11(17):3151–2.

56. Patel S, Doble BW, MacAulay K, Sinclair EM, Drucker DJ, Woodgett JR. Tissue-Specific Role of Glycogen Synthase Kinase 3β in Glucose Homeostasis and Insulin Action. Mol Cell Biol. 2008 Oct 15;28(20):6314–28.

57. DeFronzo RA, Tripathy D. Skeletal muscle insulin resistance is the primary defect in type 2 diabetes. Diabetes Care. 2009 Nov;32 Suppl 2:S157-163.

58. Lamb GD, Cellini MA. High intracellular [Ca2+] alters sarcoplasmic reticulum function in skinned skeletal muscle fibres of the rat. J Physiol. 1999 Sep 15;519 Pt 3:815–27.

59. Lamb GD, Junankar PR, Stephenson DG. Raised intracellular [Ca2+] abolishes excitation-contraction coupling in skeletal muscle fibres of rat and toad. J Physiol. 1995 Dec 1;489 (Pt 2):349–62.

60. Verburg E, Murphy RM, Richard I, Lamb GD. Involvement of calpains in Ca2+-induced disruption of excitation-contraction coupling in mammalian skeletal muscle fibers. Am J Physiol Cell Physiol. 2009 May;296(5):C1115-1122.

61. Place N, Ivarsson N, Venckunas T, Neyroud D, Brazaitis M, Cheng AJ, et al. Ryanodine receptor fragmentation and sarcoplasmic reticulum Ca2+ leak after one session of high-intensity interval exercise. Proc Natl Acad Sci. 2015 Dec 15;112(50):15492–7.

62. Ashida Y, Himori K, Tamai K, Kimura I, Yamada T. Preconditioning contractions prevent prolonged force depression and Ca2+-dependent proteolysis of STAC3 after damaging eccentric contractions. J Appl Physiol Bethesda Md 1985. 2021 Nov 1;131(5):1399–407.

63. Otani K, Han DH, Ford EL, Garcia-Roves PM, Ye H, Horikawa Y, et al. Calpain system regulates muscle mass and glucose transporter GLUT4 turnover. J Biol Chem. 2004 May 14;279(20):20915–20.

64. Dowling JJ, Lawlor MW, Dirksen RT. Triadopathies: an emerging class of skeletal muscle diseases. Neurother J Am Soc Exp Neurother. 2014 Oct;11(4):773–85.

65. Lawal TA, Todd JJ, Witherspoon JW, Bönnemann CG, Dowling JJ, Hamilton SL, et al. Ryanodine receptor 1-related disorders: an historical perspective and proposal for a unified nomenclature. Skelet Muscle. 2020 Nov 16;10(1):32.

66. Leon LR, Bouchama A. Heat stroke. Compr Physiol. 2015 Apr;5(2):611–47.

67. Hopkins PM, Ellis FR, Halsall PJ. Evidence for related myopathies in exertional heat stroke and malignant hyperthermia. Lancet Lond Engl. 1991 Dec 14;338(8781):1491–2.

68. Turner RM, Pirmohamed M. Statin-Related Myotoxicity: A Comprehensive Review of Pharmacokinetic, Pharmacogenomic and Muscle Components. J Clin Med. 2019 Dec 20;9(1):22.

69. Brushia RJ, Walsh DA. Phosphorylase kinase: the complexity of its regulation is reflected in the complexity of its structure. Front Biosci J Virtual Libr. 1999 Sep 15;4:D618-641.

70. Henriksen EJ, Dokken BB. Role of glycogen synthase kinase-3 in insulin resistance and type 2 diabetes. Curr Drug Targets. 2006 Nov;7(11):1435–41.

71. Dokken BB, Henriksen EJ. Chronic selective glycogen synthase kinase-3 inhibition enhances glucose disposal and muscle insulin action in prediabetic obese Zucker rats. Am J Physiol Endocrinol Metab. 2006 Aug;291(2):E207-213.

72. Maqbool M, Hoda N. GSK3 Inhibitors in the Therapeutic Development of Diabetes, Cancer and Neurodegeneration: Past, Present and Future. Curr Pharm Des. 2017 Nov 16;23(29):4332–50.

73. Singh RB, Chohan PK, Dhalla NS, Netticadan T. The sarcoplasmic reticulum proteins are targets for calpain action in the ischemic-reperfused heart. J Mol Cell Cardiol. 2004 Jul;37(1):101–10.

74. Singh RB, Hryshko L, Freed D, Dhalla NS. Activation of proteolytic enzymes and depression of the sarcolemmal Na+/K+-ATPase in ischemia-reperfused heart may be mediated through oxidative stress. Can J Physiol Pharmacol. 2012 Feb;90(2):249–60.

75. Guo A, Zhang C, Wei S, Chen B, Song LS. Emerging mechanisms of T-tubule remodelling in heart failure. Cardiovasc Res. 2013 May 1;98(2):204–15.

76. Wu CC, Chen B, Jiang Y, Jia Z, Martin DW, Liu S, et al. Calpain-Dependent Cleavage of Junctophilin-2 and T-Tubule Remodeling in a Mouse Model of Reversible Heart Failure. J Am Heart Assoc. 3(3):e000527.

77. Boucher J, Kleinridders A, Kahn CR. Insulin Receptor Signaling in Normal and Insulin-Resistant States. Cold Spring Harb Perspect Biol. 2014 Jan;6(1):a009191.

78. Hesselbarth N, Kunath A, Kern M, Gericke M, Mejhert N, Rydén M, et al. Repin1 deficiency in adipose tissue improves whole-body insulin sensitivity, and lipid metabolism. Int J Obes 2005. 2017 Dec;41(12):1815–23.

79. Zhu X, Li H, Wu Y, Zhou J, Yang G, Wang W. lncRNA MEG3 promotes hepatic insulin resistance by serving as a competing endogenous RNA of miR-214 to regulate ATF4 expression. Int J Mol Med. 2019 Jan;43(1):345–57.

80. Murphy RM, Snow RJ, Lamb GD. mu-Calpain and calpain-3 are not autolyzed with exhaustive exercise in humans. Am J Physiol Cell Physiol. 2006 Jan;290(1):C116-122.

81. Murphy RM, Goodman CA, McKenna MJ, Bennie J, Leikis M, Lamb GD. Calpain-3 is autolyzed and hence activated in human skeletal muscle 24 h following a single bout of eccentric exercise. J Appl Physiol. 2007 Sep;103(3):926–31.

82. Zhang HB, Li RC, Xu M, Xu SM, Lai YS, Wu HD, et al. Ultrastructural uncoupling between T-tubules and sarcoplasmic reticulum in human heart failure. Cardiovasc Res. 2013 May 1;98(2):269–76.

83. Perni S, Beam KG. Voltage-induced Ca2+ release is supported by junctophilins 1, 2 and 3, and not by junctophilin 4. J Gen Physiol. 2022 Sep 5;154(9):e2021ecc22.

84. Censier K, Urwyler A, Zorzato F, Treves S. Intracellular calcium homeostasis in human primary muscle cells from malignant hyperthermia-susceptible and normal individuals. Effect Of overexpression of recombinant wild-type and Arg163Cys mutated ryanodine receptors. J Clin Invest. 1998 Mar 15;101(6):1233–42.

85. Pouvreau S, Royer L, Yi J, Brum G, Meissner G, Ríos E, et al. Ca(2+) sparks operated by membrane depolarization require isoform 3 ryanodine receptor channels in skeletal muscle. Proc Natl Acad Sci U S A. 2007 Mar 20;104(12):5235–40.

86. Manno C, Figueroa LC, Gillespie D, Fitts R, Kang C, Franzini-Armstrong C, et al. Calsequestrin depolymerizes when calcium is depleted in the sarcoplasmic reticulum of working muscle. Proc Natl Acad Sci U S A. 2017 Jan 24;114(4):E638–47.

87. Launikonis BS, Zhou J, Royer L, Shannon TR, Brum G, Ríos E. Confocal imaging of [Ca2+] in cellular organelles by SEER, shifted excitation and emission ratioing of fluorescence. J Physiol. 2005 Sep 1;567(Pt 2):523–43.

88. Zhou J, Yi J, Royer L, Launikonis BS, González A, García J, et al. A probable role of dihydropyridine receptors in repression of Ca2+ sparks demonstrated in cultured mammalian muscle. Am J Physiol Cell Physiol. 2006 Feb;290(2):C539-553.

89. Figueroa L, Shkryl VM, Zhou J, Manno C, Momotake A, Brum G, et al. Synthetic localized calcium transients directly probe signalling mechanisms in skeletal muscle. J Physiol. 2012 Mar 15;590(Pt 6):1389–411.

90. Van Der Voort HTM, Strasters KC. Restoration of confocal images for quantitative image analysis. J Microsc. 1995 May 1;178(2):165–81.

91. Agard DA, Hiraoka Y, Shaw P, Sedat JW. Fluorescence microscopy in three dimensions. Methods Cell Biol. 1989;30:353–77.

92. Messerli JM, van der Voort HT, Rungger-Brändle E, Perriard JC. Three-dimensional visualization of multi-channel volume data: the amSFP algorithm. Cytometry. 1993 Oct;14(7):725–35.

93. Bolte S, Cordelières FP. A guided tour into subcellular colocalization analysis in light microscopy. J Microsc. 2006 Dec;224(Pt 3):213–32.

94. Sikkel MB, Francis DP, Howard J, Gordon F, Rowlands C, Peters NS, et al. Hierarchical statistical techniques are necessary to draw reliable conclusions from analysis of isolated cardiomyocyte studies. Cardiovasc Res. 2017 Aug;113(14):1743–52.

Acknowledgments

We are grateful to Prof. Manuel Díaz, for discussion and comments — akin to mentoring — on many aspects of this study, to Prof. Filip Van Petegem for helpful suggestions (notably, that multiple cuts in JPh1 may be needed to release the regulatory fragment), to Prof. Vincenzo Sorrentino, for his generous gift of an N-terminal Myc-tagged junctophilin1 vector, to Profs. Isabelle Marty and Graham Lamb, for detailed comments on the manuscript and its prepublication in bioRxiv. Funding: National Institute of Arthritis and Musculoskeletal and Skin Diseases (R01 AR 071381) to S.R., E.R., and M. Fill (Rush University). National Institute of Arthritis and Musculoskeletal and Skin Diseases (R01 AR 072602) to E.R., S. L. Hamilton, S. Jung and F. Horrigan (Baylor College of Medicine). National Center for Research Resources (S1055024707) to E.R. and others.

Competing Interests

None.